CHALMERS
FINITE ELEMENT CENTER

PREPRINT 2001–18

Adaptive finite element methods for incompressible fluid flow

Johan Hoffman and Claes Johnson

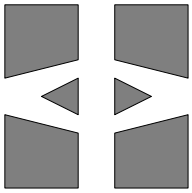

Chalmers Finite Element Center
CHALMERS UNIVERSITY OF TECHNOLOGY
Göteborg Sweden 2002

CHALMERS FINITE ELEMENT CENTER

Preprint 2001–18

Adaptive finite element methods for incompressible fluid flow

Johan Hoffman and Claes Johnson

CHALMERS

Chalmers Finite Element Center
Chalmers University of Technology
SE–412 96 Göteborg Sweden
Göteborg, January 2002

Adaptive finite element methods for incompressible fluid flow
Johan Hoffman and Claes Johnson
NO 2001–18
ISSN 1404–4382

Chalmers Finite Element Center
Chalmers University of Technology
SE–412 96 Göteborg
Sweden
Telephone: +46 (0)31 772 1000
Fax: +46 (0)31 772 3595
www.phi.chalmers.se

Printed in Sweden
Chalmers University of Technology
Göteborg, Sweden 2002

ADAPTIVE FINITE ELEMENT METHODS FOR INCOMPRESSIBLE FLUID FLOW

JOHAN HOFFMAN AND CLAES JOHNSON

ABSTRACT. We present recent work on the following issues of CFD: (i) discretization of the non-stationary incompressible Navier-Stokes equations, (ii) solution of the discrete system at each time step, (iii) hydrodynamic stability, (iv) adaptive error control and a posteriori error estimates, (v) transition to turbulence and (vi) turbulence modeling.

1. INTRODUCTION

The Navier-Stokes equations give the basic model for fluid flow and describe a variety of phenomena in hydro and aero-dynamics, processing industry, biology, oceanography, meteorology, geophysics and astrophysics. Fluid flow may contain features of *incompressible* and *compressible* flow, *Newtonian* and *non-Newtonian* flow, and *turbulent* and *laminar* flow, with turbulent flow being irregular with rapid fluctuations in space and time and laminar flow being more organized. *Computational Fluid Dynamics* CFD concerns the simulation of fluid flow by solving the Navier-Stokes equations numerically. The basic issues of CFD is *computability* relating to errors from numerical computation, and *predictability* relating to errors from imprecision in given data. The basic question for a given flow situation may be formulated as follows: what quantity can be computed/predicted to what tolerance to what cost? We emphasize the *quantitative* aspects concerning both the choice of quantity to compute, the error tolerance and the computational cost. We may expect a turbulent flow to be more computationally demanding than a laminar flow, and a pointwise quantity (e.g the viscous stresses at a specific point) more demanding than an average quantity (e.g. the drag or lift).

In these notes we give a survey of our recent work on this question, continuing in particular our AGARD 92 lecture notes [15], with focus on adaptive finite element methods for non-stationary incompressible Newtonian laminar and beginning turbulent flow with medium large Reynolds numbers in the range $100 - 1000$. The basic issues entering are the following: (i) discretization of the incompressible Navier-Stokes equations, (ii) solution of the discrete system at each time step, (iii) hydrodynamic stability, that is the growth of

Date: January 24, 2002.

Key words and phrases. incompressible flow, a posteriori error estimation, hydrodynamic stability, turbulence modeling, multi adaptivity, dynamic subgrid modeling, wavelets.

Department of Mathematics, Chalmers University of Technology, S–412 96 Göteborg, Sweden, *email*: hoffman@math.chalmers.se, claes@math.chalmers.se

These notes were prepared for the von Karman Institute Lecture Series: Error estimation and solution adaptive discretization i Computational Fluid Dynamics, Nasa-Ames Sept 10–15, VKI Oct 15–19, 2001.

errors/perturbations from computation/data, (iv) adaptive error control and a posteriori error estimates, (v) transition to turbulence and (vi) turbulence modeling. We now give an introductory overview of the basic topics (i)-(vi). For an overview of adaptive finite element methods including references, we refer to the survey articles [2] and [1], see also [4] and [5], containing many details on various aspects of finite element adaptivity omitted in these notes. For an overview of finite element methods for the incompressible Navier-Stokes equations including references, we refer to [23]. For a survey of turbulence modeling we refer to [6], [27] and [8] and references therein.

1.1. **Discretization.** To discretize the Navier-Stokes equations to get a discrete system of equations on each time step, we use the general stabilized Galerkin/least squares space-time finite element method developed over the years together with Hughes, Tezduyar and coworkers. With continuous piecewise polynomials in space of order p and discontinuous or continuous piecewise polynomials in time of order q, we refer to this method as cG(p)dG(q) or cG(p)cG(q). In the computations presented in these notes we use cG(1)cG(1) with continuous piecewise linears in space for both velocity and pressure on tetrahedral meshes and Crank-Nicolson time stepping. Discretization introduces *discretization errors* containing Galerkin piecewise polynomial approximation errors and quadrature errors. For turbulent flow, some form of *turbulence modeling* is necessary, introducing also a *modeling error*. We may view the discretization and modeling error together to form the *computational error*.

1.2. **Discrete solvers.** The discrete system in velocity-pressure on each time step is solved using a fixed point/defect correction outer iteration, and for the corresponding inner iteration linear system we use GMRES in the velocity with the pressure solved in terms of the velocity using a multigrid Poisson solver. We also perform the inner iteration with defect correction in the velocity with given pressure. This method is efficient and robust for the non-stationary medium Reynolds number flows considered in these notes. The discrete solver introduces additional discretization errors from approximate solution of the discrete equations.

1.3. **Hydrodynamic stability.** Hydrodynamic stability concerns the stability features of a given solution of the Navier-Stokes equations (base flow), that is the growth of perturbations from data or computation in a given flow. Hydrodynamic stability features may be expressed by different *stability factors* measuring the growth of different perturbations/errors from data, modeling or discretization. The Galerkin discretization error basically has the form of a product of *residuals* connecting to *interpolation errors* depending on the smoothness of the solution, and related stability factors. The stability factors may be computed by numerically solving linearized (forward or dual backward) Navier-Stokes equations with appropriate data, linearized at (an approximation of) the base flow. Stability factors normally increase with increasing *Reynolds number* $Re = \frac{UL}{\nu}$, where U is a reference velocity, L is a reference length, and ν is the *kinematic viscosity*, and with increasing time scale T. The Reynolds number Re may range from small (of size 1) for very viscous flows, to very large (up to 10^9 or more) in aero or hydro-dynamics, with turbulent flow often appearing for Re larger than $10^2 - 10^3$. The stability factors may vary from

small (of size 1) to medium (size 10^2 say) to large. Stability factors may grow linearly with KT for laminar flow, and (momentarily) exponentially with KT for pointwise quantities in turbulent flow, where K is a measure of the velocity gradient. Typically, K is small for laminar flow (outside layers) and large for turbulent flow (locally of the order $Re^{3/4}$), and T is typically large (of the order Re) for laminar flow. Fluid dynamics with Re medium/large, which is our main focus here, thus usually has KT medium/large, with stability factors growing linearly with KT for laminar flow and (momentarily) exponentially for pointwise quantities in turbulent flow. Turbulent flow thus has non-smooth solutions and large stability factors for pointwise quantities, and thus is pointwise uncomputable in the sense that the required mesh size would be too small (smaller than say 10^{-3} on the unit cube) and thus require too many operations and too much memory for todays computers. The aim of *turbulence modeling* is to compute solution averages which are smoother and have smaller stability factors using feasible mesh sizes (say 10^{-2} on the unit cube). The process of turbulence modeling introduces a *modeling error*, which together with the discretization error forms the total computational error.

1.4. **Adaptivity and a posteriori error estimates.** We present here a general approach to adaptive error control based on a posteriori error estimates. We then consider a mathematical model of the form $A(u) = f$, where A is a *differential operator*, f is given *data*, and u is the *solution*. The model is subject to perturbations from *data* represented by $\hat{f}$, *modeling* represented by $\hat{A}$, and *discretization* represented by U viewed as a numerical approximate solution to a perturbed problem $\hat{A}(\hat{u}) = \hat{f}$ with exact solution $\hat{u}$, with U obtained using a Galerkin finite element method. We say that the *data/modeling error* is equal to $u - \hat{u}$ and the *discretization error* is equal to $\hat{u} - U$, and that the total error $u - U = u - \hat{u} + \hat{u} - U$, thus has a contribution from data/modeling and a contribution from discretization. The model perturbation $\hat{A}$ may represent a turbulence model in applications to fluid flow.

An *adaptive method* for solving $A(u) = f$ includes a *feed-back process*, where the quality of computed solutions U of perturbed models $\hat{A}(\hat{u}) = \hat{f}$, are investigated with the objective of decreasing the modeling error $u - \hat{u}$ by improving the model $\hat{A}$, and/or the discretization error $\hat{u} - U$, the latter typically by appropriately modifying the local mesh size. An adaptive method is based on *a posteriori error estimates* estimating the data/modeling and discretization errors in terms of computable residuals such as $f - A(U)$ or $\hat{f} - \hat{A}(U)$, or estimated residuals such as $f - A(\hat{u})$.

Adaptive feed-back in modeling and discretization may be viewed as one aspect of *optimization* with the objective of decreasing the modeling and discretization errors. Adding also aspects of optimization of solutions, which is often the main objective, one gets a full picture of solution optimization including optimization of modeling and discretization. This problem is of the same general form with now the equation $A(u) = f$ representing a Lagrange system of equations characterizing solution optimality.

We now present the key steps in the derivation of an a posteriori error estimate for the discretization error in a Galerkin finite element method for the equation $\hat{A}(\hat{u}) = \hat{f}$ of the

form: Find $U \in V$ such that $(\hat{A}(U), v) = (\hat{f}, v)$ for $v \in V_h$, where V_h is a finite dimensional subspace, on a mesh with mesh size h, of a Hilbert space V with scalar product $(\cdot, \cdot)$ and norm $\|\cdot\|$, and $\hat{A} : V \to V$ is Frechet differentiable with derivative $A' : V \to V$. Supposing that we want to estimate the quantity (e, ψ) where $e = \hat{u} - U$ and ψ is a given element in V, we write

$$\begin{aligned} \hat{A}(\hat{u}) - \hat{A}(U) &= \int_0^1 \frac{d}{ds}\hat{A}(s\hat{u} + (1-s)U)\, ds \\ &= \int_0^1 A'(s\hat{u} + (1-s)U)\, ds\, e \equiv A'(\hat{u}, U)e, \end{aligned}$$

and let $\varphi \in V$ be the solution to the *dual linearized problem* $(A'(\hat{u}, U)w, \varphi) = (w, \psi)$ for all $w \in V$, and obtain choosing $w = e$ the following *error representation*

$$(e, \psi) = (A'(\hat{u}, U)e, \varphi) = (\hat{A}(\hat{u}) - \hat{A}(U), \varphi) = (\hat{f} - \hat{A}(U), \varphi) = (\hat{R}(U), \varphi),$$

in terms of the residual $\hat{R}(U) = \hat{f} - \hat{A}(U)$. We then use *Galerkin orthogonality* to obtain, with $\Phi \in V_h$ an interpolant of φ satsifying an *interpolation error estimate* of the form $\|h^{-2}(\varphi - \Phi)\| \leq C_i \|D^2\varphi\|$,

$$(e, \psi) = (\hat{R}(U), \varphi - \Phi) \leq C_i \|h^2 \hat{R}(U)\|\, \|D^2\varphi\| \leq C_i S \|h^2 \hat{R}(U)\|\, \|\psi\|,$$

where D^2 represents a second derivative, $h(x,t)$ is the local mesh size, $S = \frac{\|D^2\varphi\|}{\|\psi\|}$ is a stability factor and C_i an interpolation constant. Normalizing ψ, we obtain an a posteriori error estimate of the form

$$|(e, \psi)| \leq C_i S \|h^2 \hat{R}(U)\|$$

estimating the error in terms of the residual $\hat{R}(U)$, the mesh size h and the stability and interpolation factors S and C_i. The interpolation factor C_i only depends on the finite elements used, while we have to compute the dual problem, depending on both u and U and ψ, to get the stability factor S.

An *adaptive method* typically involves a *stopping criterion* guaranteeing that the error measure is less than a given tolerance, and a *modification strategy* to be applied if the stopping criterion is not satisfied. Both the stopping criterion and modification strategy may be based on an a posteriori error estimates of the form just given, involving the residuals $f - A(U)$ and $\hat{f} - \hat{A}(U)$ of computed solutions, and/or *a priori* error estimates involving estimates of the exact solution $\hat{u}$ or u, and including appropriate stability factors. A modification strategy may concern quantities related to discretization such as the local mesh size, or quantities related to turbulence modeling such as turbulent viscosities. The modification strategy for the local mesh size is often based on *equidistribution* with the objective of satisfying the stopping criterion with a minimal number of degrees of freedom, or largest possible local mesh size.

The dual problem is linearized at a mean value of the exact solution u and the computed solution U. In practice, when solving the dual problem to compute stability factors, we have to replace u by U and thus linearize at the computed solution U. In order for the corresponding linearization effect to be small, we expect to require U to approximate u

pointwise sufficiently well. We return to this issue shortly in the context of turbulence modeling, where U may be expected to be a pointwise approximation to a local average u^h of u, but not u itself. It appears natural to choose the size of the average so that the discretization and modeling errors balance, with the discretization error decreasing and the modeling error increasing with increasing averaging.

1.5. **Transition to turbulence.** The phenomenon of transition from laminar to turbulent flow, studied intensively by Reynolds more than hundred years ago in the case of pipe flow, has long been an outstanding open problem in science, where today computational methods shed new light. Reynolds observed by injecting dye into water flowing through a transparent pipe, that sometimes the flow changed quite abruptly from organized laminar to turbulent fluctuating flow at some point downstream from the inlet, with the transition being identified by the deviation of the dye from a straight line into a rapidly fluctuating path. Seemingly similar sudden changes may be observed in the raising smoke from a cigarett, or in a stock market crash, or a sudden break up of a long-lasting marriage.

The basic question in all these cases is: why does the transition take place at a specific point in space or time, or not at all? Observing the straight line of the dye in Reynolds experiment before the transition, does not appear to give any signal of emerging instability, and a stock market crash necessarily must be a surprise for the majority of the market actors. The research on transition to turbulence in fluid flow has largely focussed on finding a relation between the Reynolds number and transition, with ideally a so called critical Reynolds number for each type of flow, identified by the fact that transition to turbulence takes place if and only if the actual Reynolds number is larger than the critical Reynolds number. Reynolds himself had little reason to belive in the existence of such critical Reynolds numbers noting that in his own experiments the transition took place in one pipe and not in another at the same Reynolds number. Nevertheless, most text books in fluid mechanics today present critical Reynolds numbers for various flows, such as 5772 for Pouiseuille flow between two parallel fixed plates (with parabolic velocity profile), and ∞ for Couette flow between two moving parallel plates (with linear velocity profile), both however at severe variance with experiments. For example, Couette flow may go turbulent in experiments for a wide range of Reynolds numbers starting at around 300, depending on the experimental set-up, and similarly Pouiseuille flow starting around 1000. The stated critical Reynolds numbers come out of a so called normal mode stability analysis of 2d linearized equations, referred to as the Orr-Sommerfeld equations, based on identifying exponentially growing eigenmodes. The striking difference in the theoretical predictions and the practical experiments for transition in parallel flow, has driven the classical study of hydrodynamic stability into a severe crisis.

However, during the last decades new insight on the importance of 3d perturbations and non-modal growth has been developing, see [26], giving a better understanding of the process of transition from laminar to turbulent flow in almost parallel flow, such as pipe flow and boundary layer flow. We will present pieces of this new picture as an application of a quantitative mathematical/computational analysis of hydrodynamic stability. In particular, the analysis will show that even if the dye injected into the pipe indicates

that fluid particles follow (almost) straight lines prior to the transition, the flow actually gets considerably reorganized as a necessary preparation before the transition. We will refer to the reorganization as resulting from the *Taylor-Görtler mechanism* through which small transversal velocity perturbations after some time result in big perturbations in the streamwise velocity, which is the initial and crucial phase of the transition process, and which results from the non-normality of the linearized Navier-Stokes equations when linearized at parallel flow. Of course we may expect to find similar reorganizations preparing transitions into stock market and marriage crashes.

A possible reason for the survival of the classical misleading normal mode stability analysis for parallel flow, despite its lack of experimental support, is probably the fact that there are some other cases, where the same type of analysis in fact is correct and conforms with experiments, namely the *bifurcating* Benard and Taylor-Couette flows, changing from one configuration to another at a certain well defined Reynolds number. The bifurcation of Bernard flow involves the development of organized patterns of convective rolls of fluid in motion. A bifurcation involves a change from one configuration loosing stability, to a new stable configuration, which is different from the process of transition to turbulence, with the new configuration being increasingly unstable. Now, a bifurcation in general may be detected through a normal mode analysis based on finding for the linearized equations an eigenvalue with zero real part. In particular, the critical Reynolds number for the first bifurcations in Taylor-Couette and Bernard flow, may be found analytically this way. As indicated this approach does however not work for parallel Couette or Poiseuille flow, which do not bifurcate to find new stable configurations, but instead go into turbulent unstable motion. It appears that the success of the mathematical theory in the bifurcating cases, has overshadowed the failure in the non-bifurcating cases.

1.6. **Turbulence modeling.** The design of *turbulence models* has been a major open problem in fluid mechanics since the initial efforts in this direction by Reynolds at end of the 19th century. Turbulent flow appears to be pointwise uncomputable on todays computers because of the presence of small-scale features and large stability factors. The basic problem of *turbulence modeling* is to represent the effects of the unresolved scales on resolvable scales in computable models. Today, computational methods open new possibilities of approaching this fundamental problem of mathematical modeling, in the form of *Dynamic Large Eddy Simulation* DLES, where the the turbulence model is constructed as a part of the computational process with dynamic feed-back from the computation.

The problem of turbulence modeling may be described as follows: Let u^h be an approximation of the exact solution u corresponding to a local running average of size h representing the finest computationally resolvable scale. We seek to compute a pointwise accurate approximation U of u^h using a mesh of size h, in a situation where a pointwise accurate approximate solution of the exact solution u itself would be impossible because u contains significant scales finer than h (unresolvable subgrid scales with effects on the resolvable scales). We start seeking an equation satisfied by u^h by making an Ansatz of the form $A(u^h) + A(u)^h - A(u^h) = f^h$, where we need to approximate $F_h(u) \equiv A(u)^h - A(u^h)$ in terms of u^h in a *subgrid model* $\hat{F}_h(u^h)$, with thus $\hat{F}_h(u^h)$ an approximation of $F_h(u)$, to

get a model of the form $\hat{A}(\hat{u}) = A(\hat{u}) + \hat{F}_h(\hat{u}) = f^h = \hat{f}$. The quantity $F_h(u)$ has the form of a (generalized) *covariance* and we thus face a problem of modeling covariances. In the setting of the Navier-Stokes equations, the term $F_h(u)$ corresponds to (derivatives of) the exact *Reynolds stresses*, and the turbulence modeling problem is to find an expression $\hat{F}_h(u^h)$ approximating $F_h(u)$ in terms of u^h. Having determined a turbulence model in the form of a function $\hat{F}_h$, we solve the Galerkin equation: Find $U \in V_h$ such that $(A(U) + \hat{F}_h(U), v) = (\hat{f}, v)$ for all $v \in V_h$. The total error will then connect to a modeling residual $F_h(u) - \hat{F}_h(U)$ and a discretization residual $A(U) + \hat{F}_h(U) - \hat{f}$ in a posteriori error estimates, where the modeling residual has to be approximated by extrapolation, while the discretization residual is directly computable from U.

The problem of turbulence modeling thus may be viewed to be to construct the function $\hat{F}_h$. The basic approaches use *similarity models* based on extrapolation from coarser scales assuming a scale regularity, or *turbulent viscosity models* with the Reynolds stresses approximated as viscous resolvable stresses given by a *turbulent viscosity*, or *mixed models* with a combination of similarity and turbulent viscosity models.

We now return to the question of linearization in connection to a posteriori error estimates, assuming the approximate solution U to be a pointwise accurate approximation of u^h, but not the turbulent solution u itself, because of unresolvable subgrid scales. Aiming then at an a posteriori error estimate for $u^h - U$, we will have a modeling error contribution from the quantity $F_h(u)$, and we will need to estimate this quantity even if we do not use a turbulence model. Using a turbulence model with $\hat{F}_h(U)$ an approximation of $F_h(u)$, we instead need to estimate $F_h(u) - \hat{F}(U)$. At any rate, we need to estimate or model $F_h(u)$. With the terminology used above, we view the turbulence modeling error as a part of the total computational error with ideally a balance of discretization and modeling errors.

2. The incompressible Navier-Stokes equations

The incompressible Navier-Stokes equations expressing conservation of momentum and incompressibility of a unit density constant temperature Newtonian fluid with constant kinematic viscosity $\nu > 0$ enclosed in a volume Ω in $\mathbb{R}^3$, take the form: find (u, p) such that

$$\begin{aligned} D_{u,t}u - \nu\Delta u + \nabla p &= f && \text{in } \Omega \times I, \\ \operatorname{div} u &= 0 && \text{in } \Omega \times I, \\ u &= w && \text{on } \partial\Omega \times I, \\ u(\cdot, 0) &= u^0 && \text{in } \Omega, \end{aligned} \tag{2.1}$$

where $u(x,t) = (u_i(x,t))$ is the *velocity* vector and $p(x,t)$ the *pressure* of the fluid at (x,t), and f, w, u^0, $I = (0,T)$, is a given driving force, Dirichlet boundary data, initial data and time interval, respectively. Further,

$$D_{u,t}v = \dot{v} + (u \cdot \nabla)v \tag{2.2}$$

is the *particle derivative* of $v(x,t)$ measuring the rate of change $\frac{d}{dt}v(x(t),t)$ of $v(x(t),t)$ along the trajectory $x(t)$ of a fluid particle with velocity u, satisfying $\dot{x}(t) = u(x(t),t)$,

where as usual $\dot{v} = \partial v/\partial t$. The quantity $\nu\Delta u - \nabla p$ represents the total fluid force, and may alternatively be expressed as

$$\nu\Delta u - \nabla p = \operatorname{div}\sigma(u,p), \tag{2.3}$$

where $\sigma(u,p) = (\sigma_{ij}(u,p))$ is the *stress tensor*, with components $\sigma_{ij}(u,p) = 2\nu\epsilon_{ij}(u) - p\delta_{ij}$, composed of the *stress deviatoric* $2\nu\epsilon_{ij}(u)$ with zero trace and an isotropic pressure: Here $\epsilon_{ij}(u) = (u_{i,j} + u_{j,i})/2$ is the *strain tensor*, with $u_{i,j} = \partial u_i/\partial x_j$, and δ_{ij} is the usual Kronecker delta, the indices i and j ranging from 1 to 3. A Neumann type boundary condition, corresponding to the boundary stress being prescribed, takes the form $\sigma\cdot n = g$, where $(\sigma\cdot n)_i = \sum_j \sigma_{ij}n_j$ and $g = (g_i)$ is a given boundary stress with g_i the force component in the x_i-direction.

In the model (2.1) we assume that the *temperature* T is constant. In the general case with variable density ρ and temperature T, (2.1) is modified by replacing $D_{u,t}$ by $\rho D_{u,t}$, and adding the following equations expressing conservation of mass and energy:

$$\begin{aligned} D_{u,t}\rho &= 0 \qquad \text{in } \Omega\times I,\\ D_{u,t}T - \nabla\cdot(\mu\nabla T) &= F \qquad \text{in } \Omega\times I, \end{aligned} \tag{2.4}$$

together with boundary and initial conditions, where μ is a heat conduction coefficient and F a heat source, assuming the heat capacity is equal to one. We note that since $\nabla\cdot u = 0$, we have $D_{u,t}\rho = \dot{\rho} + \nabla\cdot(\rho u) = 0$, which is the usual equation expressing mass conservation.

We assume that (2.1) is normalized so that the reference velocity and typical length scale are both equal to one. The Reynolds number Re is then equal to ν^{-1}. Of course, the specification of the length scale may not be very obvious and thus the Reynolds number may not have a very precise quantitative meaning.

2.1. **Existence and uniqueness of solutions.** Existence and uniqueness of solutions of the 3d incompressible Navier-Stokes equations (2.1) is an outstanding open problem in the mathematical literature, now on the Clay Institute's list of $\$10^6$ prize problems. One may argue, that little progress has been made on this problem since the work by Leray [20] from 1934 proving existence, but not uniqueness, of a certain type of weak solution. In contrast, it is known that for various so called regularized Navier-Stokes equations, existence and uniqueness of classical solutions may be proved mathematically using standard techniques from the theory of partial differential equations and functional analysis, see [9]. A common regularization consists in replacing the constant viscosity ν by the modified viscosity

$$\hat{\nu} = \nu + h^2|\epsilon(u)|^2, \tag{2.5}$$

depending on the strain $\epsilon(u)$ and the positive regularization parameter h, representing a smallest possible spatial scale. The regularization introduces a modification of the viscosity for highly strained flows, away from the Newtonian constant viscosity. In this model the basic energy estimate (assuming $f = w = 0$) obtained by multiplying the momentum equation by u and integrating:

$$\int_\Omega |u(x,T)|^2\,dx + 4\int_0^T\int_\Omega \left(\nu|\epsilon(u)|^2 + h^2|\epsilon(u)|^4\right)dx\,dt \le \int_\Omega |u^0|^2\,dx,$$

is strong enough to prove uniqueness using a standard Grönwall type argument based on a Sobolev inequality of the form

$$(w \cdot \nabla u, w) \leq C\|\nabla w\|^{3/2}\|w\|^{1/2}\|\epsilon(u)\| \leq \frac{\nu}{2}\|\nabla w\|^2 + \frac{C}{\nu^3}\|\epsilon(u)\|^4\|w\|^2,$$

with $(\cdot,\cdot)$ and $\|\cdot\|$ appropriate $L_2(\Omega)$-scalar products/norms, $w = u - v$ the difference of two solutions u and v, and C a constant of moderate size. The resulting estimate of the difference (perturbation) $w(t)$ has the form

$$\|w(t)\|^2 \leq C\exp(\frac{Ct}{h^2\nu^3})\|w(0)\|^2.$$

We note that the growth factor is extremely large in the case of main interest with ν and h small, which puts doubts to the physical meaningfulness of the uniqueness proof. If a similar mathematical uniqueness proof was possible for the limiting case of the Navier-Stokes equations with $h = 0$, which would seem to give the Clay prize, it would most likely suffer from the same presence of enormous constants, and the value of the proof could be seriously questioned.

The uniqueness question is of course intimately connected to hydrodynamic stability, which concerns the growth of perturbations (such as $w(t)$ in the above discussion) in the Navier-Stokes equations. Only solutions which are stable in some sense may be expected to exist as observable flows. Hydrodynamic stability has a long tradition going back to Reynolds, Rayleigh and Lord Kelvin, but offers surprisingly few concrete results of significance. In general, both the perturbation growth and the complexity of the flow increases with increasing Reynolds number (decreasing viscosity), with eventually the flow becoming turbulent with very strong perturbation growth and very fine scales developing. We shall show below that for even for basic types of parallel laminar flow, the growth of perturbations may be linear in the Reynolds number, indicating that the 3d Euler equations, corresponding to vanishing viscosity, cannot have any meaning.

3. Hydrodynamic stability

Hydrodynamic stability concerns the quantitative stability properties of the incompressible Navier-Stokes equations, which are of basic importance for both error control in computation and modeling, and for the understanding of phenomena of fluid flow such as bifurcation or transition to turbulence. The basic study of hydrodynamic stability concerns the linearized Navier-Stokes equations for perturbations (φ, q) of a given solution (u, p) of (2.1) corresponding to the initial data u_0 and right hand side f, obtained by subtracting (u, p) from the solution $(u + \varphi, p + q)$ corresponding to the perturbed initial data $u^0 + \varphi^0$ and right hand side $f + g$, and omitting the quadratic perturbation term $(\varphi \cdot \nabla)\varphi$:

$$\begin{aligned} D_{u,t}\varphi + (\varphi \cdot \nabla)u - \nu\Delta\varphi + \nabla q &= g && \text{in } \Omega \times I,\\ \nabla \cdot \varphi &= 0 && \text{in } \Omega \times I,\\ \varphi &= 0 && \text{on } \partial\Omega \times I,\\ \varphi(\cdot, 0) &= \varphi^0 && \text{in } \Omega, \end{aligned} \tag{3.1}$$

where $(\varphi \cdot \nabla)u = (\sum_{j=1}^3 \varphi_j u_{i,j})_{i=1}^3$ with $v_{,j} = \partial v/\partial x_j$.

The basic question in hydrodynamic stability is to estimate the solution (φ, q) of (3.1) in various norms in terms of appropriate corresponding norms of the data (g, φ_0), for example in terms of certain *stability factors*. A basic example is given by the *weak stability factor* $S_0(u,T)$ depending on the base flow u, final time T and the perturbation φ^0, defined by

$$S_0(u,T,\varphi^0) = \frac{\|\varphi\|_I}{\|\varphi^0\|}, \tag{3.2}$$

or the factor $S_0(u,T)$ depending on the base flow u and the final time T with a maximization over all perturbations, defined by

$$S_0(u,T) = \sup_{\varphi^0 \in L_2} \frac{\|\varphi\|_I}{\|\varphi^0\|}, \tag{3.3}$$

where φ is the solution of (3.1) with $g = 0$ and initial data $\varphi^0 \neq 0$, and $\|v\| = \|v\|_{L_2(\Omega)}$, $\|v\|_I = \sup_{0<t<T} \|v(\cdot,t)\|$. The factor $S_0(u,T,\varphi^0)$ measures the growth over the time interval $(0,T)$ of the perturbation φ^0 of initial data, and the factor $S_0(u,T)$ measures the maximal growth over the time interval $(0,T)$ of an initial perturbation of initial data. We refer to these stability factors as *weak* because we measure the solution itself and not derivatives thereof. *Strong* stability factors measure derivatives of the solution of dual linearized equations, connect to Galerkin discretization errors and occur as multiplicative factors in a posteriori error estimates.

We now give estimates of the stability factor $S_0(u,T)$ in two extreme cases: a *worst case* with exponential dependence in KT related to non-smooth turbulent flow, and a *best case* with linear dependence in KT related to smooth laminar flow. The strong stability factors coupled to Galerkin discretization show the same span of variation. Assuming that $K = 1$ and $T = \nu^{-1} = Re$, the dependence can be expressed as an exponential or linear dependence in the Reynolds number Re, with the exponential dependence indicating uncomputability even for moderately large Reynolds numbers, while the linear dependence make smooth laminar flows computable.

3.1. **Worst case exponential perturbation growth.** Multiplying the first equation of (3.1) by φ and integrating over $\Omega \times (0,t)$, using the incompressibility of both u and φ, one gets for $t > 0$:

$$\|\varphi(\cdot,t)\|^2 \leq -2\int_0^t \int_\Omega (\varphi \cdot \nabla) u \cdot \varphi \, dxds + \|\varphi^0\|^2,$$

from which follows by the Grönwall inequality that $S_0(u,T) \leq \exp(CKT)$, with $C \approx 1$, which is a worst case exponential estimate. We note the exponential growth is generated by the presence of the zero order term $(\varphi \cdot \nabla)u$, as in the simple scalar ode $\dot{\psi} = K\psi$ with solution $\psi(t) = \psi(0)\exp(Kt)$. A flow with this very strong perturbation growth cannot exist as a stable flow. Since there are some more or less stable flows observable in nature, it must be possible in special cases to obtain reduced growth rates by using particular features of the zero order coupling term $(\varphi \cdot \nabla)u$. A basic such case arises in nearly parallel flow, with a particular coupling of the perturbations of the velocities in streamwise and transversal directions, which we now turn to.

3.2. **Linear perturbation growth for nearly parallel flow.** *Nearly parallel flow* is a basic type of flow, also referred to as *shear flow*, occuring in pipe flow and boundary layer flow, where the streamlines are almost parallel straight lines and the transversal variation of the streamline flow velocity is balanced by a shear force. We now show that for such flows the weak stability factor $S_0(u,T)$ defined by (3.3) satisfies $S_0(u,T) \approx KT$. This estimate underlies the first crucial step in the scenario of transition to turbulence in nearly parallel flow to be presented, showing that a perturbation growth $\approx \nu^{-1}$ over time intervals of length $T\nu^{-1}$ is possible even if for smooth flows with $K = 1$, indicating that a small initial perturbation (of size ν say) in fact may cause the base flow to change significantly if we only wait long enough (over a time interval $\approx \nu^{-1}$).

We consider a smooth parallel stationary base flow (u,p) in an infinitely long straight pipe $\Omega = \mathbb{R}\times\omega$, where ω in the (x_2,x_3)-plane is the cross-section (with smooth boundary) of the pipe of diameter of size 1, and the axis of the pipe is oriented along the x_1-axis, and u vanishes on the boundary of the pipe. We assume that the base flow (u,p) is independent of x_1 and satisfies the following assumptions

$$\|u_1\| \approx 1, \qquad \|\bar\nabla u_1\|_\infty = C, \qquad \|\bar u\|_\infty + \|\bar\nabla \bar u\|_\infty \le c\nu, \tag{3.4}$$

where $\|\cdot\|_\infty$ denotes the maximum norm, $\bar u = (u_2,u_3)$, and $\bar\nabla = (\partial/\partial x_2, \partial/\partial x_3)$ is the gradient with respect to (x_2,x_3). Here and below, c and C denote positive constants of moderate size, which are independent of ν. The assumption (3.4) including a smooth streamwise velocity $u_1 \approx 1$ in the x_1 direction being independent of x_1, and smooth small transversal velocities $\bar u$ of size $\approx \nu$, may be viewed as a basic characteristic of nearly parallel flow. A further characteristic may be that the derivatives in the streamwise direction x_1 are one order smaller in ν, so that $u_{1,1} \sim \nu$ and $u_{2,1}, u_{3,1} \sim \nu^2$. We will return to this feature below in the presentation of the scenario of transition to turbulence. We further assume as already indicated that $T \sim 1/\nu = Re$.

Assuming that also the perturbation (φ, q) are independent of x_1, the linearized equations (3.1), take the following form:

$$\begin{aligned}
D_{u,t}\varphi_1 + (\bar\varphi\cdot\bar\nabla)u_1 - \nu\Delta\varphi_1 &= 0 \qquad \text{in } \omega\times I,\\
D_{u,t}\bar\varphi + (\bar\varphi\cdot\bar\nabla)\bar u + \bar\nabla q - \nu\Delta\bar\varphi &= 0 \qquad \text{in } \omega\times I,\\
\bar\nabla\cdot\bar\varphi \equiv \varphi_{2,2} + \varphi_{3,3} &= 0 \qquad \text{in } \omega\times I,\\
\varphi &= 0 \qquad \text{on } \partial\omega\times I,\\
\varphi(\cdot,0) &= \varphi_0 \qquad \text{on } \omega.
\end{aligned} \tag{3.5}$$

These equations have a very particular structure. First, the equations for the transversal velocity $\bar\varphi$ are fully decoupled from the equation for the streamwise velocity φ_1, and have zero order terms with small coefficients because $|\bar\nabla\bar u| \le c\nu$. Secondly, the zero order term $(\bar\varphi\cdot\bar\nabla)u_1$ in the equation for φ_1 does not contain φ_1, because $u_{1,1} = 0$. This means that the zero order terms in (3.5) have a special form, which makes it possible to reduce the general worst case exponential growth of $S_0(T)$, to a linear growth. The basic structure of the equations (3.5) is present in the system of ordinary differential equations $\dot\varphi_1 - \varphi_2 = 0$, $\dot\varphi_2 = 0$, for $t > 0$, $\varphi^0 = (0,\varphi_2^0)$ with solution $\varphi_1(t) = t\varphi_2^0$, $\varphi_2(t) = \varphi_2^0$, showing a linear growth of φ_1. The growth in this system is very different from the exponential growth

obtained changing the first equation to $\dot{\varphi}_1 - \varphi_1 = 0$, with the exponentially growing solution $\varphi_1(t) = \exp(t)\varphi_1^0$, assuming now $\varphi_1^0 \neq 0$. Clearly, the change from linear to exponential growth is related to the nature of the coupling, with the direct coupling $\dot{\varphi}_1 = \varphi_1$ being much stronger than the indirect coupling $\dot{\varphi}_1 = \varphi_2$, where $\dot{\varphi}_2 = 0$.

We now prove a basic estimate giving a linear growth bound in time of the streamwise velocity perturbation φ_1 generated by a small transversal perturbation $\bar{\varphi}^0$. We refer to the physical phenomena causing this perturbation growth as the *Taylor-Görtler mechanism*, which has a crucial role in transition to turbulence. The bound is based on an energy estimate using the decoupling of φ_1 and $\bar{\varphi}$, resulting from the fact that $q_{,1} = 0$ and $\varphi_{1,1} = 0$. Below we present computations showing that the bound is sharp and that linear perturbation growth actually occurs.

Theorem 1. *The stability constant $S_0(u,T)$, defined by (3.3) in the context of x_1-independent nearly parallel pipe flow (u,p) satisfying (3.4), satisfies the following bound for $T = \nu^{-1}$:*

$$S_0(u,T) \leq C\nu^{-1}, \tag{3.6}$$

where C depends on the constant c in (3.4). If the constant c is small enough, then the estimate (3.6) holds for $T \geq \nu^{-1}$ with ν^{-1} replaced by T.

Proof. First, multiplying the equation for $\bar{\varphi}$ by $\bar{\varphi}$, and integrating over ω using the fact that $\bar{\nabla} \cdot \bar{u} = \bar{\nabla} \cdot \bar{\varphi} = 0$, shows that

$$\frac{1}{2}\frac{d}{dt}\|\bar{\varphi}\|^2 + \nu\|\bar{\nabla}\bar{\varphi}\|^2 \leq c\nu\|\bar{\varphi}\|^2.$$

Using Grönwall's inequality, we then find that

$$\|\bar{\varphi}(\cdot,t)\|^2 \leq \exp(C\nu t)\|\bar{\varphi}^0\|^2, \qquad 0 < t \leq T.$$

Next, multiplying the equation for φ_1 by φ_1 and using again the fact that $\bar{\nabla} \cdot \bar{u} = \bar{\nabla} \cdot \bar{\varphi} = 0$, we get

$$\frac{1}{2}\frac{d}{dt}\|\varphi_1\|^2 + \nu\|\bar{\nabla}\varphi_1\|^2 \leq \frac{1}{2}\nu\|\varphi_1\|^2 + \frac{1}{2}\nu^{-1}\|\bar{\varphi}\|^2,$$

from which the desired estimate follows by integration. The modification with c sufficiently small is left to the reader. □

A challenge is to extend the above result to different base flows (u,p) with slight x_1-dependence. As a small contribution to this problem we present the following example: we assume in addition to (3.4) that

$$\|u_{1,1}\|_\infty \leq c\nu, \qquad \|\bar{u}_{,1}\|_\infty \leq c\nu^2, \tag{3.7}$$

where c is a positive constant, and we allow the perturbation velocity φ to depend on x_1, but we assume for the pressure part q that $q_{,1} = 0$ and that correspondingly the incompressibility condition reduces to $\varphi_{2,2} + \varphi_{3,3} = 0$, which corresponds to a slight compressibility of the original fluid with a pressure perturbation q, which is constant in the x_1-direction.

In this case the linearized perturbation equations take the form:

$$\begin{aligned} D_{u,t}\varphi_1 + (\varphi\cdot\nabla)u_1 - \nu\Delta\varphi_1 &= 0 \quad \text{in } \Omega\times I,\\ D_{u,t}\bar\varphi + (\varphi\cdot\nabla)\bar u + \bar\nabla q - \nu\Delta\bar\varphi &= 0 \quad \text{in } \Omega\times I,\\ \varphi_{2,2}+\varphi_{3,3} &= 0 \quad \text{in } \Omega\times I,\\ \varphi &= 0 \quad \text{on } \partial\Omega\times I,\\ \varphi(\cdot,0) &= \varphi_0 \quad \text{on } \Omega, \end{aligned}$$

which again decouples and thus is amenable to analysis as above.

Remark 1. *The Orr-Sommerfeld equations are the linearized Navier-Stokes equations linearized at x_1-directed parallel flow $u=(u_1(x_2),0,0)$ between two parallel plates with normal in the x_2 direction, assuming the perturbations are independent of the transversal direction x_3 parallel to the plates and also that $\varphi_3=0$: find $(\varphi(x_1,x_2,t),p(x_1,x_2,t)$ such that for $|x_2|<d$, $x_1\in\mathbb{R}$, $t>0$*

$$\begin{aligned} \dot\varphi_1 + u_{1,2}\varphi_2 - \nu\Delta\varphi_1 + p_{,1} &= 0,\\ \dot\varphi_2 - \nu\Delta\varphi_2 + p_{,2} &= 0,\\ \varphi_{1,1}+\varphi_{2,2} &= 0, \end{aligned} \tag{3.8}$$

with $\varphi(x_1,\pm d)=0$, and the initial condition $\varphi(x_1,x_2,0)=\varphi^0(x_1,x_2)$, and where $2d$ is the distance between the plates. In the case of Couette flow $u_1(x_2)\propto x_2$ and for Pouiseuille flow $u_1(x_2)\propto(1-(x_2/d)^2)$. The stability factor $S_0(u,T)$ turns out to be much smaller than the corresponding factor for the linearized problem (3.5) with x_1 independent perturbations. We conclude that x_2-independent perturbations seem to be less significant than x_1-independent perturbations, and thus conclude that the Orr-Sommerfeld equations do not seem to be so relevant in initial transition to turbulence in nearly parallel flow.

4. Computability of the Lorenz system

The meteorologist E. Lorenz presented in his famous 1972 talk *Does the flap of a butterfly's wings in Brazil set off a tornado in Texas?*, the following 3×3-ode model of the Navier-Stokes equations with the purpose of explaining well-known uncertainties in weather prediction:

$$\begin{cases} \dot x &= \sigma(y-x),\\ \dot y &= rx - y - xz,\\ \dot z &= xy - bz, \end{cases} \tag{4.1}$$

with initial data $(x(0),y(0),z(0))=(1,0,0)$, and $\sigma=10$, $b=8/3$ and $r=28$. The solution $u(t)=(x(t),y(t),z(t))$ turns out to be very sensitive to perturbations and in our terminology thus has stability factors with very rapid (exponential) growth in time. The computational challenge is to solve the Lorenz system accurately on a time interval $[0,T]$ with T as large as possible. We present results on this question from [21], which we expect to be of some relevance also for the Navier-Stokes equations.

In Figure 1 we plot the x-component of the Lorenz system on $[0,40]$ computed using cG(q) and dG(q) with $q=1,2,3,4,5,10$ using a constant time step $k=0.001$ and double precision arithmetic. We indicate a correct solution with a solid line, and an incorrect

solution with a dashed line. We note that increasing q does not help to produce a correct solution beyond $T = 40$, nor does it help to decrease the time step. This is because at every time-step we make a relative round off error of at least 10^{-16} using double precision, and the only possibility to get beyond $T = 40$ would be to take fewer time-steps using a very high order method.

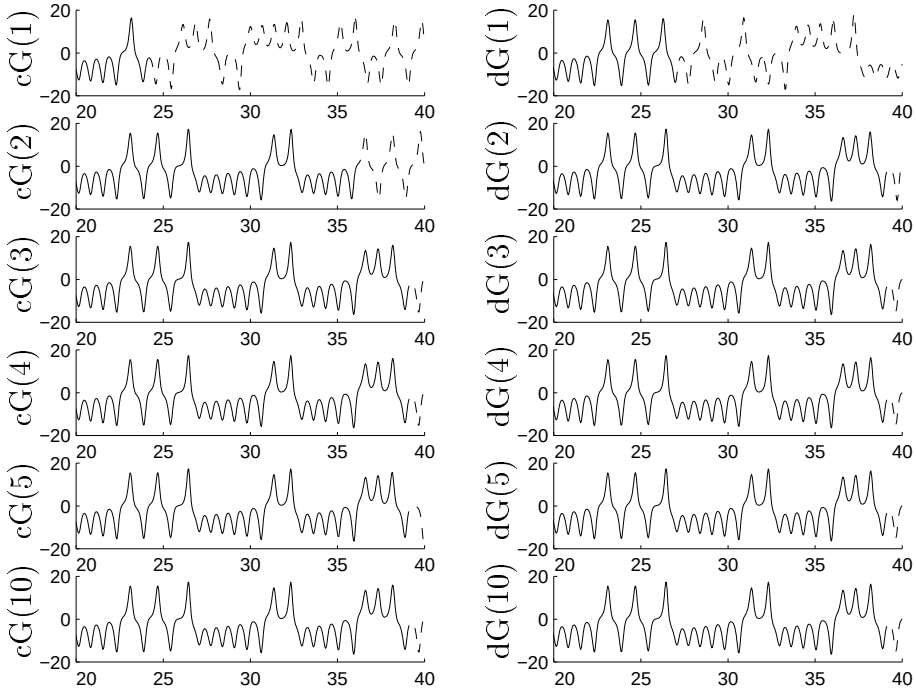

FIGURE 1. The x-component of Lorenz solutions on $[20, 40]$ computed with different methods using the constant time-step $k = 0.001$

In Figure 2 we present solutions with high order cG(q) with the larger time step $k = 0.1$, which are accurate to almost $T = 50$. Increasing the time step further does not help to get beyond $T = 50$.

In Figure 3 we plot the stability factor $S(T)$ measuring the accumulation of round-off or quadrature errors over the time interval $[0, T]$, which is computed by solving an appropriate dual linearized problem. The stability factor grows with an overall exponential rate, but the growth is different in different parts of the trajectory. We see that $S(T)$ reaches the value 10^{16} for $T = 50$, which agrees with the double precision limit found above. Computing in quadruple precision would allow accurate computation to $T = 100$.

We note that a worst case estimate using a relevant Lipschitz constant (which is of size 100), would give an upper bound of the form $S(T) \leq \exp(100T)$, indicating that we could only compute accurately to $T = 1$, which would be a gross underestimate. Even in this case with considerable exponential growth, we are far from a worst case Grönwall estimate.

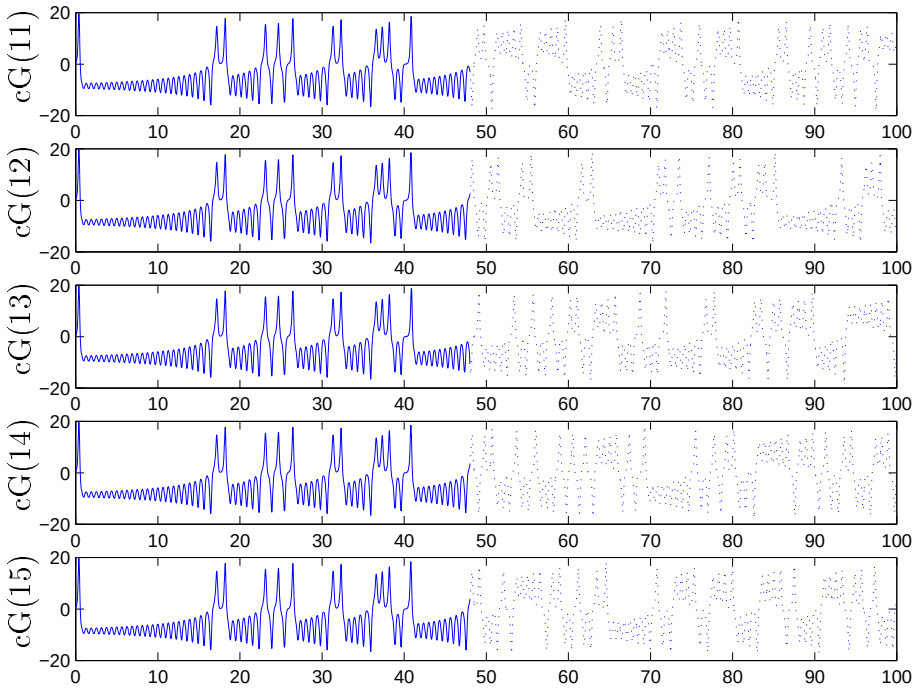

FIGURE 2. The x-component of Lorenz solutions on $[0, 50]$ computed with high-order methods using the constant time-step $k = 0.1$.

5. Discretization: General Galerkin G^2

In this section we present the general space-time Galerkin least squares stabilized finite element method, referred to as the General Galerkin G^2- method, for the incompressible Navier-Stokes equations (2.1). This method includes the *streamline diffusion method* on Eulerian space-time meshes, the *characteristic Galerkin method* on Lagrangian space-time meshes with orientation along particle trajectories, and *Arbitrary Lagrangian-Eulerian ALE methods* with different mesh orientation. Further, the least-squares stabilizations present in the G^2-method, does take care of the two difficulties traditionally met in the discretization of the incompressible Navier-Stokes equations, namely

- instabilities from Eulerian discretization of convection terms,
- pressure instabilities in equal order interpolation of velocity and pressure.

Altogether, we are able to present a general flexible methodology for the discretization of the incompressible Navier-Stokes equations applicable to a great variety of flow problems from creeping viscous flow to slightly viscous flow, including free or moving boundaries.

Let $0 = t_0 < t_1 < ... < t_N = T$ be a sequence of discrete time steps with associated time intervals $I_n = (t_{n-1}, t_n]$ of length $k_n = t_n - t_{n-1}$ and space-time slabs $S_n = \Omega \times I_n$, and let $W_n \subset H^1(\Omega)$ be a finite element space consisting of continuous piecewise polynomials of degree p on a mesh $\mathcal{T}_n = \{\kappa\}$ of mesh size $h_n(x)$ with W_{0n} the functions in W_n vanishing on Γ. To define the G^2-method for (2.1) with homogeneuos Dirichlet boundary conditions

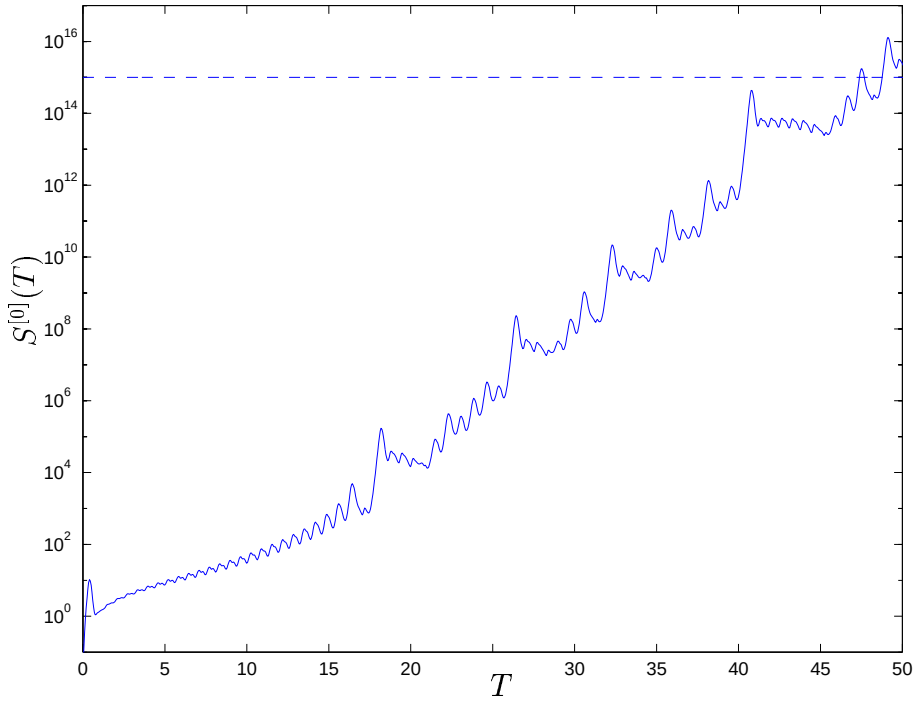

FIGURE 3. The stability factor $S(T)$ measuring accumulation of round-off and quadrature errors in the Lorenz system

for the velocity ($w = 0$), let for a given velocity field β on $S_n = \Omega \times I_n$ vanishing on $\Gamma \times I_n$, the particle paths $x(\bar{x}, \bar{t})$ be defined by

$$\begin{aligned} \frac{dx}{d\bar{t}} &= \beta(x, \bar{t}) \quad \bar{t} \in I_n, \\ x(\bar{x}, t_n) &= \bar{x}, \quad \bar{x} \in \Omega, \end{aligned} \tag{5.1}$$

and introduce the corresponding mapping $F_n^\beta : S_n \to S_n$ defined by $(x, t) = F_n^\beta(\bar{x}, \bar{t}) = (x(\bar{x}, \bar{t}), \bar{t})$, where $x = x(\bar{x}, \bar{t})$ satisfies (5.1). Define for a given $q \geq 0$, the spaces

$$\bar{V}_n^\beta = \{\bar{v} \in H^1(S_n)^3 : \bar{v}(\bar{x}, \bar{t}) = \sum_{j=0}^{q} (\bar{t} - t_n)^j U_j(\bar{x}),\ U_j \in [W_{0n}]^3\},$$

$$\bar{Q}_n^\beta = \{\bar{q} \in H^1(S_n) : \bar{q}(\bar{x}, \bar{t}) = \sum_{j=0}^{q} (\bar{t}_n - t_n)^j q_j(\bar{x}),\ q_j \in W_n\},$$

together with their analogs in (x, t)-coordinates:

$$V_n^\beta = \{v : \bar{v} \in \bar{V}_n^\beta\}, \qquad Q_n^\beta = \{q : \bar{q} \in \bar{Q}_n^\beta\}, \tag{5.2}$$

where $v(x, t) = \bar{v}(\bar{x}, \bar{t})$ and $q(x, t) = \bar{q}(\bar{x}, \bar{t})$. Defining finally $V^\beta \times Q^\beta = \prod_n V_n^\beta \times Q_n^\beta$, we can now formulate the G^2-method as follows: Find $(U, P) \in V^\beta \times Q^\beta$, such that for

$n = 1, 2, ..., N$,

$$
\begin{aligned}
&(\dot{U} + (U \cdot \nabla)U, v)_n - (P, \operatorname{div} v)_n + (q, \operatorname{div} U)_n + (2\nu\epsilon(U), \epsilon(v))_n \\
&+ (\delta_1 a(U; U, P), a(U; v, q))_n + (\delta_2 \operatorname{div} U, \operatorname{div} v)_n + ([U^{n-1}], v_+^{n-1}) \\
&= (f, v + \delta_1 a(U; v, q))_n \quad \forall (v, q) \in V_n^\beta \times Q_n^\beta,
\end{aligned} \tag{5.3}
$$

where $a(w; v, q) = D_{w,t}v + \nabla q - \nu\Delta v$ with the Laplacian defined elementwise, $\delta_1 = \frac{1}{2}(k_n^{-2} + |U|^2 h_n^{-2})^{-1/2}$ in the convection-dominated case $\nu < Uh_n$ and $\delta_1 = \kappa_1 h^2$ otherwise, $\delta_2 = \kappa_2 h$ if $\nu < Uh_n$ and $\delta_2 = \kappa_2 h^2$ otherwise, with κ_1 and κ_2 positive constants of unit size, and

$$
(v, w)_n = \int_{I_n} (v, w) dt, \quad (v, w) = \sum_{K \in \mathcal{T}_n} \int_K v \cdot w \, dx,
$$

$$
(\epsilon(v), \epsilon(w)) = \sum_{i,j=1}^{3} (\epsilon_{ij}(v), \epsilon_{ij}(w)).
$$

Further, $[v^n] = v_+^n - v_-^n$ is the jump across the time level t_n with $v_\pm^n$ the limit from $t > t_n / t < t_n$. In the Eulerian *streamline diffusion method* we choose $\beta = 0$, which means that the mesh does not move in time. The *characteristic Galerkin method* is obtained choosing $\beta = U$ (and then $\delta_1 = \kappa_1 h^2$), which means that the mesh moves with the fluid particles. We may also choose β differently which gives various versions of ALE-methods, with the mesh and particle velocity being (partly) different; for example we may move the mesh with the particle velocity at a free boundary, while allowing the mesh to move differently inside the domain.

The variational formulation (5.3) with $\delta_1 = \delta_2 = 0$ is obtained multiplying the momentum equation by v, integrating over S_n including integration by parts, and adding the incompressibility equation multiplied by q and integrating over S_n. Choosing δ_1 and δ_2 positive as indicated introduces stabilizing least-squares terms. Note that the viscous term $(2\nu\epsilon(U), \epsilon(v))_n$ may alternatively occur in the form $(\nu\nabla U, \nabla v)_n = \sum_{i=1}^3 (\nu\nabla U_i, \nabla v_i)_n$. In the case of Dirichlet boundary conditions the corresponding variational formulations will be equivalent, but not so in the case of Neumann boundary conditions, see below. Note finally that we may write the term $-(P, \operatorname{div} v)$ alternatively in the form $(\nabla P, v)$ if v vanishes on the boundary.

In extreme situations, we may add residual dependent *shock-capturing artificial viscosity*, replacing ν by $\hat{\nu} = \max(\nu, \kappa_3 |R(U, P)| h^2)$, where $R(U, P) = \sum_{i=1}^4 R_i(U, P)$ with

$$
\begin{aligned}
R_1(U, P) &= |\dot{U} + U \cdot \nabla U + \nabla P - f - \nu\Delta U|, \\
R_2(U, P) &= \nu D_2(U), \\
R_3(U, P) &= |[U^{n-1}]|/k_n \quad \text{on } S_n, \\
R_4(U, P) &= |\operatorname{div} U|,
\end{aligned} \tag{5.4}
$$

where $D_2(U)(x, t) = \max_{y \in \partial K} (h_n(x))^{-1} |[\frac{\partial U}{\partial n}(y, t)]|$ for $x \in K$, with $[\cdot]$ the jump across the element edge ∂K, and κ_3 is a positive constant of unit size. Note that $R_1(U, P)$ is defined elementwise and that with piecewise linears in space, the Laplacian ΔU is zero. In the computations presented below, we chose $\kappa_3 = 0$ corresponding to shutting off the artificial

viscosity. Note that $R_1(U,P) + R_2(U,P)$ bounds the residual of the momentum equation, with the Laplacian term bounded by the second order difference quotient $D_2(U)$ arising from the jumps of normal derivatives across element boundaries.

The special case of the Stokes equations is of course obtained omitting the nonlinear terms $(U \cdot \nabla)U$ and $(U \cdot \nabla)v$, and setting $\delta_1 = \kappa_1 h^2$, $\delta_2 = \kappa_2 h^2$. This method contains the pressure stabilizing term $(\delta_1 \nabla P, \nabla q)$, which corresponds to a weighted Laplacian equation for the pressure in terms of the velocity.

Since in the local Lagrangean coordinates $(\bar{x}, \bar{t})$ on each slab S_n with $\beta = U$,

$$\frac{\partial \bar{U}}{\partial \bar{t}} \equiv \frac{\partial}{\partial \bar{t}} U(x(\bar{x},\bar{t}),\bar{t}) = \dot{U} + U \cdot \nabla U,$$

the convection term $U \cdot \nabla U$ effectively dissappears in the characteristic Galerkin method, when expressed in the characteristic coordinates $(\bar{x}, \bar{t})$, and thus the discrete equations on each time step effectively correspond to a Stokes problem.

The order of the G^2-method with polynomials of degree p in space/time is generally $p + 1/2$, see [3]. The time stepping method in (5.3) is dG(q), the discontinuous Galerkin method with piecewise polynomials of order q, which is of order $2q+1$ seen as an ode-solver, see [21].

5.1. **Neumann boundary conditions.** If we change to Neumann boundary conditions $\sigma \cdot n = g$ on a part Γ_1 of the boundary Γ, then W_{0n} is chosen to be the functions in W_n vanishing on the remaining Dirichlet part Γ_0 of the boundary, and the right hand side is supplemented with an integral over Γ_1 of $g \cdot v$. As usual this implements the Neumann boundary condition in weak form through the presence of the term $(-P, \mathrm{div}\, v) + (2\nu\epsilon(U), \epsilon(v)) = (\sigma, \epsilon(v))$ on the left hand side, which when integrated by parts generates an integral over Γ_1 of $(\sigma \cdot n) \cdot v$. If the viscous term appears in the form $(\nu \nabla U, \nabla v)_n$ the corresponding Neumann boundary condition has the form $\nu \frac{\partial u}{\partial n} - pn = 0$, where $\frac{\partial u}{\partial n}$ is the derivative in the unit outward normal direction n.

5.2. **Outflow boundary conditions.** To simulate an outflow boundary condition we may use a Neumann condition with $g = 0$ corresponding to a zero force at outflow, simulating outflow into a large empty reservoir. The alternative condition $\nu \frac{\partial u}{\partial n} - pn = 0$ acts slightly differently as an approximation of a *transparent* outflow boundary condition.

5.3. **The Eulerian cG(1)dG(0) method.** We now consider the the G^2-method (5.3) with $p = 1$, $q = 0$ and $\beta = 0$ for (2.1), which is the Eulerian cG(1)dG(0) method with continuous piecewise linears in space (cG(1)) and piecewise constants in time (dG(0)) corresponding to the backward Euler method). We then seek an approximate velocity $U(x,t)$ such that $U(x,t)$ is continuous and piecewise linear in x for each t, and $U(x,t)$ is piecewise constant in t for each x. Similarly, we seek an approximate pressure $P(x,t)$ which is continuous piecewise linear in x and piecewise constant in t. More precisely, we seek $U^n \in V_n^0 = W_{0n}^3$ and $P^n \in Q_n^0 = W_n$ for $n = 1, ..., N$, and we define

$$\begin{aligned} U(x,t) &= U^n(x) \quad x \in \Omega, \quad t \in (t_{n-1}, t_n], \\ P(x,t) &= P^n(x) \quad x \in \Omega, \quad t \in (t_{n-1}, t_n]. \end{aligned} \tag{5.5}$$

We can now write the cG(1)dG(0) method without stabilization as follows: For $n = 1, ..., N$, find $(U^n, P^n) \in V_n^0 \times Q_n^0$ such that

$$(\frac{U^n - U^{n-1}}{k_n}, v) + (U^n \cdot \nabla U^n + \nabla P^n, v) + (\nabla \cdot U^n, q) + (\nu \nabla U^n, \nabla v) = (f^n, v) \quad \forall (v, q) \in V_n^0 \times Q_n^0, \tag{5.6}$$

The cG(1)dG(0) method with δ_1-stabilization takes the form: For $n = 1, ..., N$, find $(U^n, P^n) \in V_n^0 \times Q_n^0$ such that

$$(\frac{U^n - U^{n-1}}{k_n}, v) + (U^n \cdot \nabla U^n + \nabla P^n, v + \delta_1(U^n \cdot \nabla v + \nabla q)) + (\nabla \cdot U^n, q) + (\nu \nabla U^n, \nabla v) = (f^n, v + \delta_1(U^n \cdot \nabla v + \nabla q)) \quad \forall (v, q) \in V_n^0 \times Q_n^0, \tag{5.7}$$

where $\delta_1 = \frac{1}{2}(k_n^{-2} + |U|^2 h_n^{-2})^{-1/2}$ in the convection-dominated case $\nu < U h_n$. Note that if $k \approx \frac{h}{U}$, which is a natural choice of time step respecting a CFL-condition, then $\delta_1 \approx \frac{h}{U}$. Note that the stabilized form of the cG(1)dG(0) method is obtained by replacing v by $v + \delta_1(U^n \cdot \nabla v + \nabla q)$ in the terms $(U^n \cdot \nabla U^n + \nabla P^n, v)$ and (f^n, v). In principle, we should make the replacement throughtout, but in the present case of the cG(1)dG(0), only the indicated terms get involved because of the low order of the approximations. The perturbation in the stabilized method is of size δ_1, and thus the stabilized method has the same order as the original method (first order in h if $k \sim h$).

Letting v vary in (5.7) while choosing $q = 0$, we get the following equation (the discrete momentum equation):

$$(\frac{U^n - U^{n-1}}{k_n}, v) + (U^n \cdot \nabla U^n + \nabla P^n, v + \delta_1 U^n \cdot \nabla v) + (\nu \nabla U^n, \nabla v) = (f^n, v + \delta_1 U^n \cdot \nabla v) \quad \forall v \in V_n^0, \tag{5.8}$$

and letting q vary while setting $v = 0$, we get the following discrete "pressure equation"

$$(\delta_1 \nabla P^n, \nabla q)) = -(\delta_1 U^n \cdot \nabla U^n, \nabla q) - (\nabla \cdot U^n, q) + (\delta f^n, \nabla q) \quad \forall q \in Q_n^0. \tag{5.9}$$

The cG(1)dG(0) has a backward Euler first order accurate time stepping, and thus in general is too dissipative.

5.4. **The Eulerian cG(1)cG(1) method.** We now present the a cG(1)cG(1) variant of the above cG(1)dG(0) method using the continuous Galerkin method cG(1) in time instead of dG(0). With cG(1) in time the trial functions are continuous piecewise linear and the test functions piecewise constant. The cG(1)cG(1) variant with δ_1-stabilization reads: For $n = 1, ..., N$, find $(U^n, P^n) \in V_n^0 \times Q_n^0$ such that

$$(\frac{U^n - U^{n-1}}{k_n}, v) + (\hat{U}^n \cdot \nabla \hat{U}^n + \nabla P^n, v + \delta_1(\hat{U}^n \cdot \nabla v + \nabla q)) + (\nabla \cdot \hat{U}^n, q) + (\nu \nabla \hat{U}^n, \nabla v) = (f^n, v + \delta_1(\hat{U}^n \cdot \nabla v + \nabla q)) \quad \forall (v, q) \in V_n^0 \times Q_n^0, \tag{5.10}$$

where $\hat{U}^n = \frac{1}{2}(U^n + U^{n-1})$. This method corresponds to a second order accurate Crank-Nicolson time-stepping, but the stabilization suffers from an inconsistency up to the term

$\delta_1 \dot{u}$ resulting from the piecewise constancy of the test functions. The inconsistency seems to be be acceptable unless $\dot{u}$ is large, and we use cG(1)cG(1) in the computations presented below. The Eulerian cG(1)dG(1)-method would have consistent stabilization, but has two degrees of freedom in time per time step and thus twice as many degrees of freedom.

6. Discrete solvers

The cG(1)cG(1)-method with δ_1-stabilization leads to a system of the following principal form in each step of an outer fixed point iteration with the convection velocity being given from the previous iteration:

$$\begin{aligned} AU^n + k_n B P^n &= k_n F^n, \\ -B^\top U^n + C P^n &= G^n, \end{aligned} \tag{6.1}$$

where $A = M_n + k_n N_n - k_n \nu \Delta_n$ with M_n a mass matrix, N_n representing a discrete analog of the convection term with frozen velocity from the previous iteration, Δ_n is a discrete Laplacian, B is a discrete gradient, $B^\top$ a discrete divergence, and $C = -\delta_1 \Delta_n$. In the computations presented below we solved this system using a fixed point inner iteration, where we first solve for $P^{n,j+1}$ in terms of $U^{n,j}$ from the equation

$$C P^{n,j+1} = G^n + B^\top U^{n,j}$$

using a multigrid method, and then solve for $U^{n,j+1}$ from the equation

$$A U^{n,j+1} = k_n F^n - k_n B P^{n,j+1}$$

using GMRES. The inner iteration converges if k_n/δ_1 is small enough. Since typically $\delta_1 \approx h_n/U^n$, we need $\frac{U^n k_n}{h_n}$ to be small enough, which is a CFL-like condition.

We may also apply GMRES directly to the equation $AU^n + k_n B P^n = k_n F^n$ with P^n solved in terms of U^n from the equation $B^\top U^n + C P^n = G^n$ using multigrid. The number of GMRES iterations would then depend on the condition number of the matrix $M_n + k_n N_n - k_n \nu \Delta_n + \frac{k_n}{\delta_1} B \Delta_n^{-1} B^\top$, which is bounded with k_n/h_n, $k_n \nu / h_n^2$ and k_n/δ_1.

In both variants the full iterative procedure converges in a few iterations in our typical applications of non-stationary high Reynolds number flow with k_n/h_n and k_n/δ_1 bounded by 1.

7. A posteriori error estimates with stability weights

As an example, we now prove an a posteriori error estimate for (5.6) following our general methodology. Aiming at error control of $(e(T), \psi)$ with $e = u - U$ and $\psi \in [L_2(\Omega)]^3$ given, we introduce the following linearized dual problem: find $(\varphi, \theta) \in L_2(I; [H_0^1(\Omega)]^3 \times L_2(\Omega)) \equiv W$ such that in $Q = \Omega \times (0, T)$

$$\begin{aligned} -\dot{\varphi} - (u \cdot \nabla)\varphi + \nabla U \cdot \varphi + \nabla \theta - \epsilon \Delta \varphi &= 0 \quad && \text{in } Q \\ \operatorname{div} \varphi &= 0 \quad && \text{in } Q \\ \varphi &= 0 \quad && \text{on } \Gamma \times I, \\ \varphi(\cdot, T) &= \psi \quad && \text{in } \Omega, \end{aligned} \tag{7.1}$$

where $(\nabla U \cdot \varphi)_j = U_{,j} \cdot \varphi$. Multiplying the first equation by e, integrating over Q together with integration by parts, using that $(u \cdot \nabla)u - (U \cdot \nabla)U = (u \cdot \nabla)e + (e \cdot \nabla)U$, gives

$$
\begin{aligned}
(e(T), \psi) &= \sum_{n=0}^{N} \{(-\dot{\varphi} - (u \cdot \nabla)\varphi + \nabla U \cdot \varphi, e)_n + (\nabla\theta, e)_n + (\nu\nabla\varphi, \nabla e)_n\} \\
&= \sum_{n=1}^{N} \{(\varphi, e_t)_n + ((u \cdot \nabla)e, \varphi)_n + ((e \cdot \nabla)U, \varphi)_n \\
&\quad - (\theta, \operatorname{div} e)_n + (\epsilon\nabla\varphi, \nabla e)_n - (p - P, \operatorname{div}\varphi)_n\} + \sum_{n=1}^{N} ([U^{n-1}], \varphi_+^{n-1}) \\
&= \sum_{n=1}^{N} \{(\dot{u} + u \cdot \nabla u + \nabla p, \varphi)_n + (\epsilon\nabla u, \nabla\varphi)_n \\
&\quad - (\dot{U} + U \cdot \nabla U + \nabla P, \varphi)_n - (\epsilon\nabla U, \nabla\varphi)_n \\
&\quad + (\theta, \operatorname{div} U)_n\} + \sum_{n=1}^{N} ([U^{n-1}], \varphi_+^{n-1}) \\
&= -\sum_{n=1}^{N} \{(\dot{U} + U \cdot \nabla U + \nabla P - f, \varphi - \Phi)_n \\
&\quad - (\nu\nabla U, \nabla(\varphi - \Phi))_n + (\operatorname{div} U, \theta - \Theta)_n\} + \sum_{n=1}^{N} ([U^{n-1}], \varphi_+^{n-1} - \Phi_+^{n-1}).
\end{aligned}
$$

Estimating now the interpolation errors $\varphi - \Phi$ and $\theta - \Theta$, and recalling the definition (5.4), we obtain an estimate of the form

$$
\begin{aligned}
|(e(T), \psi)| \le \sum_{i=1}^{3} \int_Q R_i(U)(Ch^m |D^m\varphi| + Ck|\dot{\varphi}|)dx\,dt \\
+ \int_Q R_4(U)(Ch^m |D^m\theta| + Ck|\dot{\theta}|)dx\,dt,
\end{aligned} \tag{7.2}
$$

for $m = 1, 2$, where D^m measures derivatives with respect to x of order m, and C represents interpolation constants. To get a concrete a posteriori error estimate, we solve the dual problem numerically and compute approximations of the derivatives of the dual solution involved. With adaptive choice of meshing, we choose $h_n(x)$ and k_n from a principle of equidistribution with the derivatives of the dual solution entering as weights.

8. A posteriori error estimates with stability factors

In the a posteriori error estimate (7.2), certain derivatives of the the dual solution appear as a weights in a space time integral over the residuals R_i. We may estimate the space-time

integral in various ways; for instance using Cauchy's inequality with $L_2(I;(L_2(\Omega))$-norms $\|\cdot\|_I$ with $I=[0,T]$, we obtain an a posteriori error estimate of for example the form

$$
\begin{aligned}
|(e(T),\psi)| &\le C\|\dot\varphi\|_I \sum_{=1}^{3} \|kR_i(U,P)\|_I \\
&+ C\|D^2\varphi\|_I \sum_{i=1}^{3} \|h^2 R_i(U,P)\|_I \\
&+ C\|\dot\theta\|_I \|kR_4(U,P)\|_I + C\|D^1\theta\|_I \|hR_4(U,P)\|_I
\end{aligned}
\tag{8.1}
$$

with $\|\dot\varphi\|_I$, $\|D^2\varphi\|_I$, $\|\dot\theta\|_I$ and $\|D^1\theta\|_I$ entering as multiplicative *stability factors*. The equidistribution now works on e.g. the product kR_1 with a mesh size factor and a residual factor.

9. Computation of lift and drag

Suppose we want to compute an approximation of the quantity

$$
N(\sigma(u,p)) = \frac{1}{T}\int_0^T \int_{\Gamma_1} \sum_{i,j=1}^{3} \sigma_{i,j}(u,p) n_j \psi_i \, ds,
\tag{9.1}
$$

where $\Gamma = \Gamma_0 \cup \Gamma_1$ is a decomposition of the boundary Γ, and $\psi=(\psi_i)$ is a given function on Γ_1, and (u,p) solves (2.1). The quantity $N(\sigma)$ may represent the mean value over $[0,T]$ of the drag or lift on a body with boundary Γ_1 immersed in a flow, depending on the choice of ψ with for example $\psi_1=\psi_2=0, \psi_3=1$ to give the lift if the x_3 is oriented vertically (and $u_3\approx 0$). Instead of directly using (9.1), we may use the following alternative expression with the idea of increasing the precision, see [7],

$$
N(\sigma(u,p)) = \frac{1}{T}\int_0^T (\dot u + u\cdot\nabla)u, \psi) - (p, \operatorname{div}\psi) + (2\nu\epsilon(u), \epsilon(\psi))) \, dt,
$$

where ψ is an extension of the given ψ into Ω with $\psi=0$ on Γ_0, which follows by integrating by parts in the last two terms, and using the momentum equation for the solution (u,p). We see that the representation does not depend on the particular extension of ψ being used. We are thus led to approximate $N(\sigma(u,p))$ by the quantity

$$
N_h(\sigma(U,P)) = \frac{1}{T}\int_0^T ((\dot U + U\cdot\nabla)U, \Psi) - (P, \operatorname{div}\Psi) + (2\nu\epsilon(U), \epsilon(\Psi))) \, dt
$$

where Ψ is a finite element function satisfying $\Psi=\psi$ on Γ_1, assuming ψ is the restriction to Γ_1 of a finite element function and (U,P) is a finite element solution of (2.1). Again, the discrete momentum equation shows that $N_h(\sigma(U,P))$ is independent of the extension Ψ. Let now (φ,θ) be the solution of the linearized dual problem $\varphi(T)=0$ and $\varphi(\cdot,t)=\psi$ on Γ_1 and $\varphi(\cdot,t)=0$ on Γ_0 for $t\in[0,T]$. Reasoning as above we then obtain an a posteriori error estimate for $N(\sigma(u,p)) - N_h(\sigma(U,P))$ of the same form as (8.1) with corresponding associated stability factors.

TABLE 1. Stability factors, where $\|\cdot\|_I$ corresponds to the $L_1(I;L_1(\Omega))$-norm

$S_{0,1}$	$S_{0,2}$	$S_{1,1}$	$S_{1,2}$	$S_{1,3}$	$S_{1,4}$
$\|\varphi\|_I$	$\|\theta\|_I$	$\|\nabla\varphi\|_I$	$\|\dot{\varphi}\|_I$	$\|\nabla\theta\|_I$	$\|\dot{\theta}\|_I$

10. Gallery of stability factors and dual problems

In this section we present computed stability factors for a set of problems including flow around a bluff body, drag of a bluff body, channel flow with a step down and a channel flow with jets. The dual solution carries information on the growth and propagation of perturbations, and in particular underlies the mesh selection in adaptive methods, and we present plots of some dual solutions below. The dual solution may be vastly different depending on the data of the dual problem, with smooth data corresponding to large mean values. We present a selection of stability factors using the $L_1(0,T;L_1(\Omega))$-norm in space-time, denoted by $\|\cdot\|_I$ with $I=[0,T]$, for the dual solution corresponding to $L_\infty(0,T;L_\infty(\Omega))$ for the residuals, see Tab. 1. A variety of combinations of norms in space/time for the residuals and the dual solution are possible. The purpose of computing stability factors is to get a rough measure of relevant stability features. For more precise error estimation, the form of the a posteriori error estimates with (more or less local) stability weights, is advantageous.

We compute on tetrahedral meshes with mesh size $h=1/32-1/64$, and the viscosity ν varies from 10^{-3} to 10^{-4}. The stabilization introduces a numerical vicosity, which may be of size $h^{3/2}$ at best, indicating that we compute with effective viscosities in the range 10^{-2} to 10^{-3}. We note that in this study we have linearized the dual problems at computed approximations of the primal solutions averaged over a regular tetrahedral mesh of size $h=1/16$, which in the case of a highly irregular primal solution might lead to an under estimation of the stability factors.

10.1. **Bluff body.** We consider channel flow with no slip walls in a 1×1 rectangular cross section of length 4 containing a cubic body of side length 0.25 with center at $(0.5,0,0)$, where $x=0$ is the inflow boundary. We impose a parabolic inflow condition $u=(16y(1-y)z(1-z),0,0)$, a transparant outflow condition, and we set $\nu=10^{-3}$. We compute on a regular tetrahedral mesh, with $h=1/32$, using the cG(1)cG(1)-method. We start from $u=0$ at time $t=0$, and we compute to time $T=20$. We consider the problem of computing the space-time average of u_1 over the domain $\omega\times[T-d(\omega),T]$, where $\omega\subset\Omega$ is a cube centered at $(2.5,0.5,0.5)$ with side length $d(\omega)$. To estimate this error the appropriate data to the linearized dual problem is zero final data and a force $\psi=(\chi_\omega/(d(\omega)|\omega|),0,0)$ acting during the time interval $[T-d(\omega),T]$, with $\chi_\omega$the characteristic function of ω and $|\omega|$ the volume of ω. We give stability factors corresponding to a computation starting at $t=12$ for different $d(\omega)$ in Tab. 2.

The residuals are of order 1, and the product of mesh size and stability factor increases with decreasing $d(\omega)$. This example supports our belief that pointwise quantities are more

TABLE 2. Bluff body: stability factors

$d(\omega)$	$S_{0,1}$	$S_{0,2}$	$S_{1,1}$	$S_{1,2}$	$S_{1,3}$	$S_{1,4}$
1/16	6.0	3.4	121.1	33.1	16.3	57.7
1/8	4.9	3.1	78.6	19.2	12.1	35.8
1/4	3.3	2.6	46.2	11.2	7.8	18.1
1/2	1.7	1.9	20.0	5.2	3.7	8.7

TABLE 3. Step down: stability factors

$d(\omega)$	$S_{0,1}$	$S_{0,2}$	$S_{1,1}$	$S_{1,2}$	$S_{1,3}$	$S_{1,4}$
1/8	30.9	16.2	836.8	124.0	138.4	278.4
1/4	22.9	4.2	533.4	39.0	48.9	46.8
1/2	10.8	2.4	220.3	10.5	16.1	25.2

difficult to compute than mean values. In Fig.5 we note the decrease in the dual solution with (backward) time for $d(\omega)$ when the initial data is convected out of the computational domain, indicating that the error in the mean value of the solution over the time interval $[20 - d(\omega), 20]$ is independent of the error in the solution for $t < 15$ in this case.

10.2. **Step down.** We consider now a channel with no slip walls and 1×1 rectangular cross section of length 4, and a step down of height and length 0.5. We have a parabolic inflow condition $u = (64(1 - y)(y - 0.5)z(1 - z), 0, 0)$, and we use a transparent outflow condition. We set $\nu = 10^{-3}$, and we compute on a regular tetrahedral mesh, with $h = 1/32$, using the cG(1)cG(1)-method. We start from $u = 0$ at time $t = 0$, and during the start up phase we can follow the formation of the recirculation zone behind the step and also the formation of a corresponding zone where the flow separates from the top boundary.

We consider the problem of computing a space-time average over the time interval $[9, 10]$and a spatial cube $\omega \subset \Omega$ centered at $(1.5, 0.5, 0.5)$with side length $d(\omega)$, starting the computation at $t = 5$. The residuals are of order 0.1, and in Fig.3 we present stablity factors corresponding to different $d(\omega)$.

10.3. **Drag of Bluff body.** We reconsider the bluff body problem with now the objective of computing the average of the drag force over a time interval $[12, 20]$. The corresponding data for the dual problem is a boundary condition $u = (1, 0, 0)$ on the faces of the bluff body. The stability factors for this averaged quantity is several orders of magnitude less than for the more local quantities again supporting the idea that averaged quantities are easier to compute. We also note that the norm of the dual solution after an initial (backwards in time) growth approaches a stable value, see Fig.8. The corresponding dual solution is

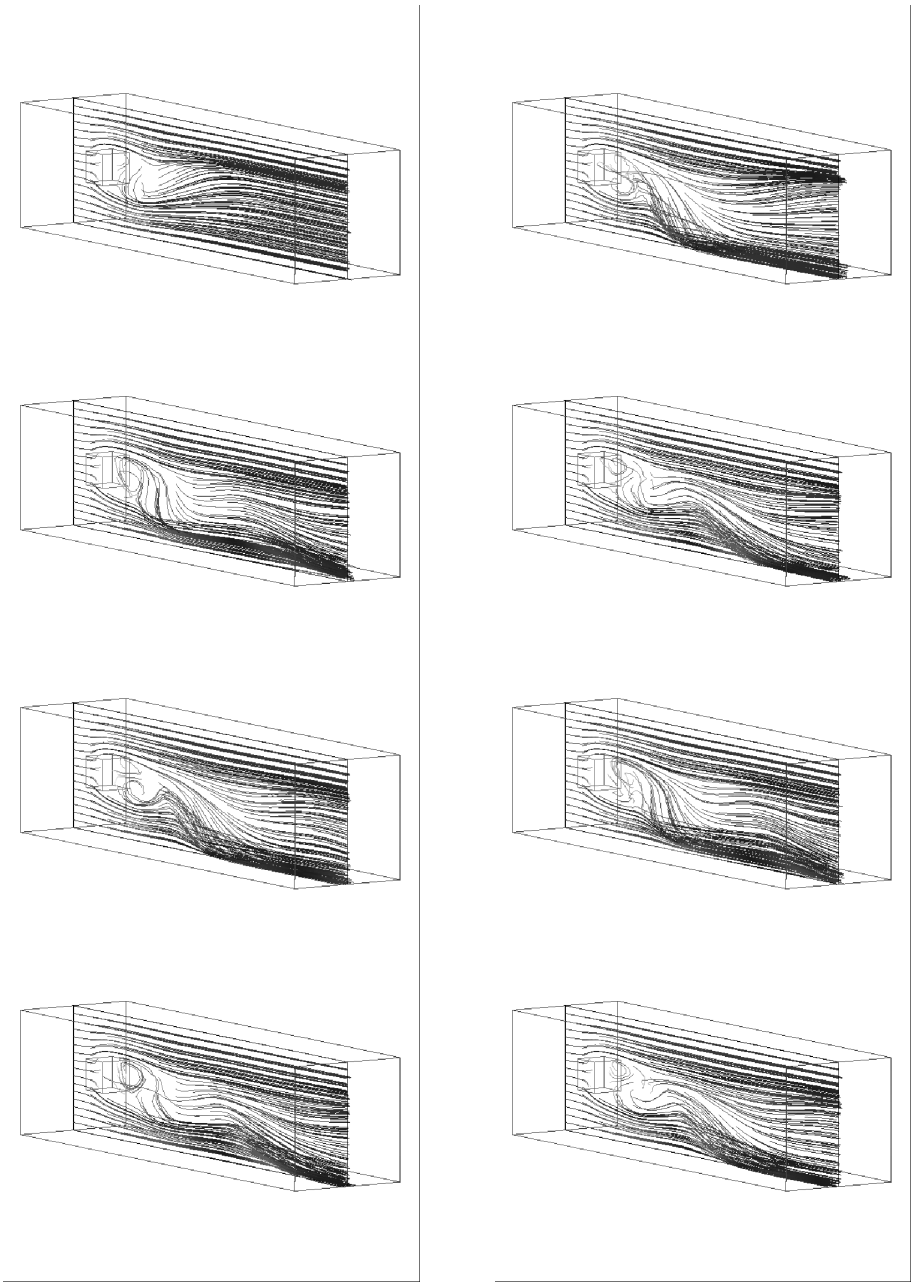

FIGURE 4. Time evolution for the Bluff body problem with $t = 2, 4, ..., 16$

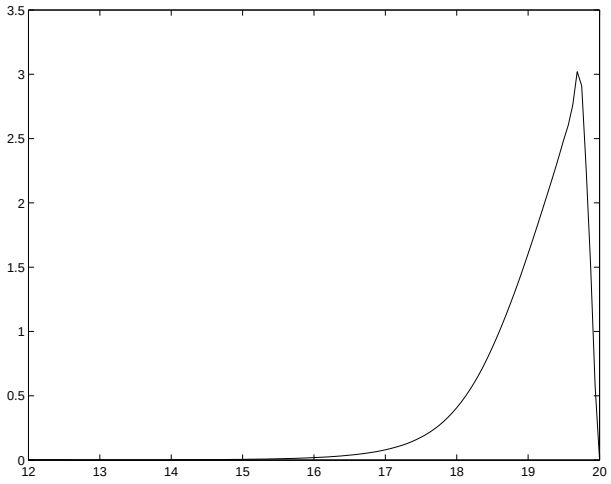

FIGURE 5. Bluff body: $\|\varphi\|_1$ for $d(\omega) = 1/4$.

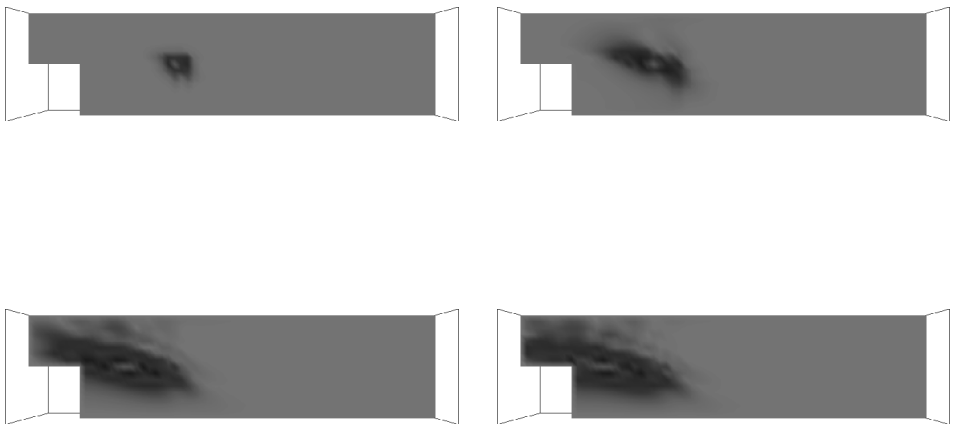

FIGURE 6. Dual solution for Step down problem for $d(\omega) = 1/8$, and backward time.

shown in Fig.9. The dual solution does not go to zero as in the previous cases, indicating (not very surprising) that the computation of a time average is dependent of the quality of the solution during the whole time interval, in contrast to the previous cases in Section 10.1-10.2 where the dependence of the quality of the solution for previous time was decreasing with (backward) time.

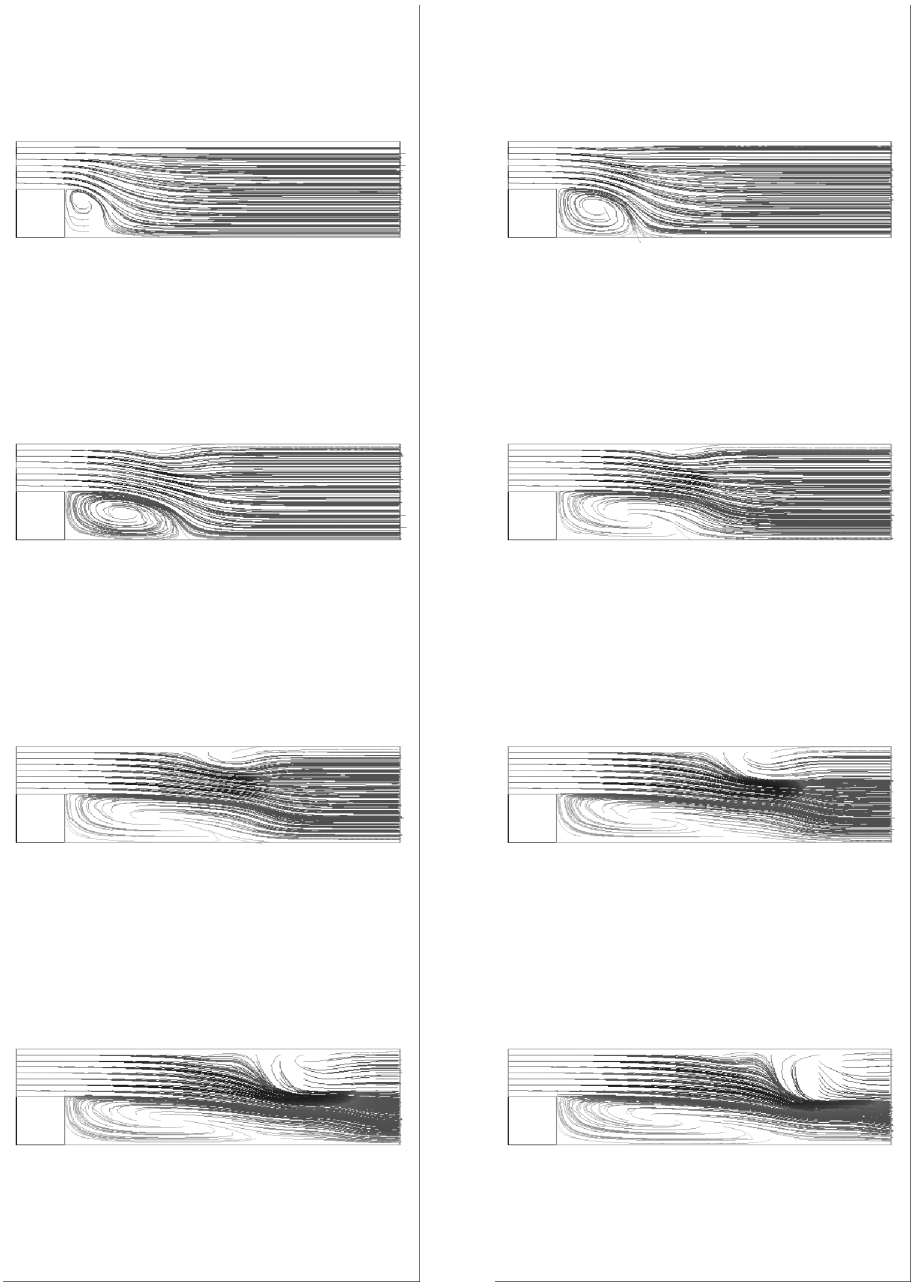

FIGURE 7. Time evolution for the Step down problem with $t = 1, 2, ..., 8$

TABLE 4. Bluff body drag: stability factors

$S_{0,1}$	$S_{0,2}$	$S_{1,1}$	$S_{1,2}$	$S_{1,3}$	$S_{1,4}$
0.13	0.11	1.6	0.03	0.43	0.06

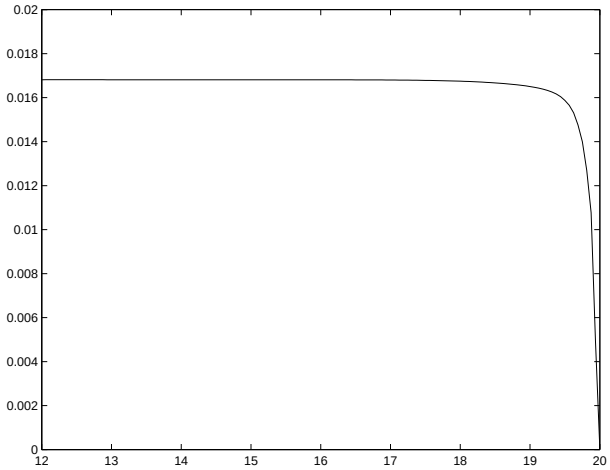

FIGURE 8. Bluff body: $\|\varphi\|_1$ for the drag problem.

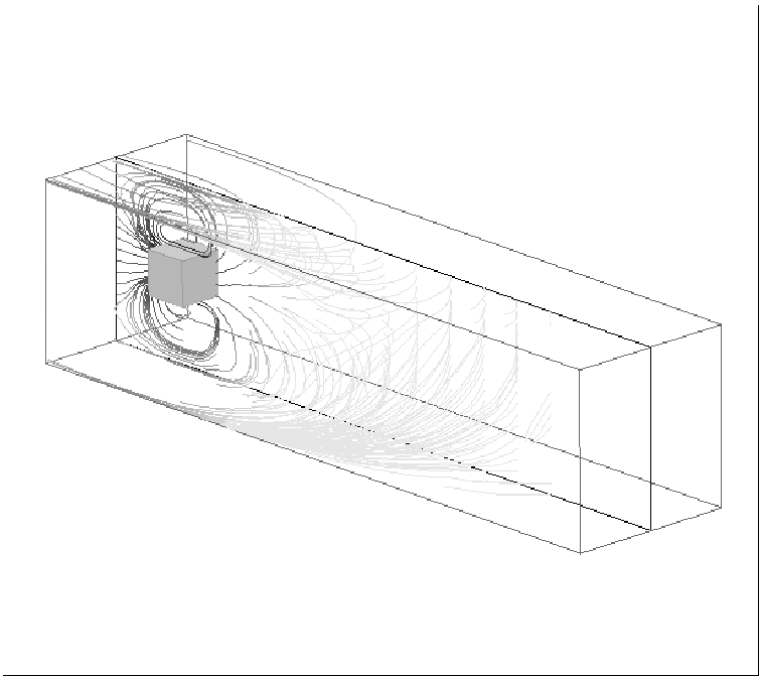

FIGURE 9. Dual solution for the Drag problem at $t = 19$

TABLE 5. Jets: stability factors corresponding to a space-time average over $\omega \times [T_0, 10]$, with $d(\omega) = 0.125$.

T_0	$S_{0,1}$	$S_{0,2}$	$S_{1,1}$	$S_{1,2}$	$S_{1,3}$	$S_{1,4}$
1/4	4.2	4.2	189.4	28.7	31.7	39.5
1/2	3.0	2.9	101.9	8.6	14.0	12.4

10.4. **Jets.** We consider a channel with no slip walls and 1×1 rectangular cross section of length 4 with an obstacle with four quadratic holes of size 0.25 at $(0.5, 0, 0)$. We have a parabolic inflow condition and we use a transparant outflow condition. The inflow condition causes the flow to form 4 high velocity jets through the holes, and in the domain behind the obstacle we get a highly irregular flow pattern. We compute on a tetrahedral mesh, with $h = 1/32$, locally refined to $h = 1/64$ for $0.125 \leq x_1 \leq 1.125$, and $\nu = 10^{-4}$, using the cG(1)cG(1)-method. We start from $u = 0$ at time $t = 0$, and we compute to time $t = 10$. The residuals are of order 1, and in In Tab. 5 we consider the case of computing a space-time average over the spatial cube ω with $d(\omega) = 0.125$ for different time intervals $[T_0, 10]$, and we find that we get larger stability factors for the shorter time interval. We then fix the time interval to $[9, 10]$and vary the side length $d(\omega)$ of the spatial cube ω, resulting in larger stability factors for smaller $d(\omega)$, see Tab. 6.

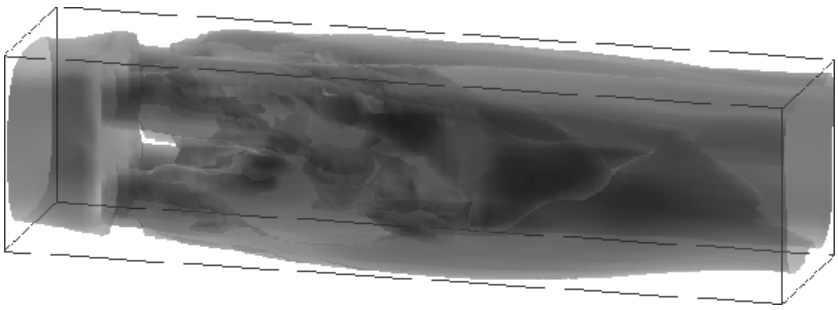

FIGURE 10. Jet problem isosurfaces at time $t = 10$.

11. The characteristic Galerkin method for free boundary flow

The characteristic Galerkin method is ideally suited to handle flow problem with free boundaries moving with the fluid, or moving boundaries with prescribed motion: just let the nodes on the fluid boundary move according to (5.1) with U a computed or prescribed velocity. We present the chG-method for the Navier-Stokes equations for a moving blob of incompressible fluid with zero stress on the entire boundary. Denoting the volume occupied by the fluid at time t by $\Omega(t)$, with $\Omega(0)$ a given initial volume, the equations read: find

TABLE 6. Jets: stability factors corresponding to a space-time average over $\omega \times [9, 10]$, with side length $d(\omega)$.

$d(\omega)$	$S_{0,1}$	$S_{0,2}$	$S_{1,1}$	$S_{1,2}$	$S_{1,3}$	$S_{1,4}$
1/16	5.2	5.5	189.8	13.0	21.1	23.1
1/8	5.0	5.4	164.7	12.1	20.0	22.9
1/4	4.1	5.0	115.6	7.8	15.2	19.0
1/2	2.3	4.0	55.9	3.6	8.5	7.9

(u, p) such that for $t \in (0, T)$,

$$\begin{aligned} \dot{u} + (u \cdot \nabla)u - \operatorname{div} \sigma &= f \quad \text{in} \quad \Omega(t), \\ \operatorname{div} u &= 0 \quad \text{in} \quad \Omega(t), \\ \sigma(u, p) \cdot n &= 0 \quad \text{on} \quad \Gamma(t), \\ u(\cdot, 0) &= u_0 \quad \text{in} \quad \Omega(0), \end{aligned} \tag{11.1}$$

where $\Gamma(t)$ is the boundary of $\Omega(t)$ with outward normal $n = n(t) = (n_j(t))$. In this problem the fluid volume $\Omega(t)$ is unknown, and is the image of the initial volume $\Omega(0)$ given by $\Omega(t) = \{x(\chi, t) : \chi \in \Omega(0)\}$, where $x(\chi, t)$ denote particle paths satisfying $\frac{dx}{dt} = u(x, t), \quad t > 0, \ , x(\bar{x}, 0) = \bar{x}$.

The characteristic Galerkin method for (11.1) based on the piecewise polynomial space W_n with no restriction on the boundary, can now be formulated as follows: find $(U, P) \in V^U \times Q^U$ such that

$$\begin{aligned} &(\dot{U} + (U \cdot \nabla U)U, v)_n - (P, \operatorname{div} v)_n + (q, \operatorname{div} U)_n + (2\nu\epsilon(U), \epsilon(v))_n \\ &+\delta_1(a(U; U, P), a(U; v, q))_n + (\delta_2 \operatorname{div} U, \operatorname{div} v)_n + \\ &\delta_3 < \sigma(u, p) \cdot n, \sigma(v, q) \cdot n >_n \\ &= (f, v + \delta_1(a(U; v, q))_n \quad \forall (v, q) \in V_n^U \times Q_n^U, \end{aligned} \tag{11.2}$$

where

$$\begin{aligned} (v, w)_n &= \int_{I_n} \int_{\Omega_h(t)} v \cdot w dx dt \\ < v, w >_n &= \int_{I_n} \int_{\Gamma_n(t)} v \cdot w ds dt, \end{aligned}$$

where $\Omega_h(t)$ with boundary $\Gamma_h(t)$ is given by $\Omega_h(t) = \{x(\bar{x}, t) : \bar{x} \in \Omega(0)\}$ with $x(\bar{x}, t)$ satisfying $\frac{dx}{dt} = U(x, t)$ for $t > 0$, and $x(\bar{x}, 0) = \bar{x} \in \Omega(0)$. In this case $\mathcal{T}_n$, is a triangulation of $\Omega_h(t_{n-1})$. We note that stress zero boundary condition is enforced weakly and that the δ_3-term gives an least squares control of the discrete boundary stress. The integrals are to interpreted as sums of integrals over the elements as usual.

In Fig 11 we present computational results by Thomas Svedberg for a 2d sloshing tank problem using the characteristic Galerkin method.

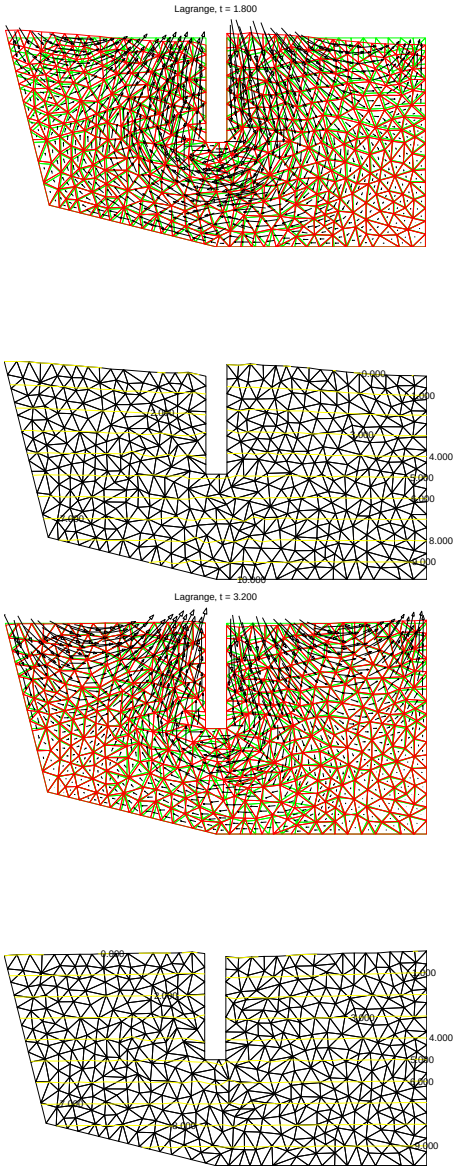

FIGURE 11. Sloshing tank computation using the characteristic Galerkin method

In the ALE method the mesh nodes on the boundary move with the particle velocity, while the nodes inside the domain move differently, for example according to an elastic string model with the nodes connected with elastic strings which amounts to solving a discrete Laplace equation. In this method interior mesh tangling is avoided.

12. TRANSITION TO TURBULENCE IN PARALLEL FLOW

In this section we present aspects of transition to turbulence in parallel flow including a simple model for transition in pipe flow, and computational results for pipe flow and

Couette flow. As a general reference into the large literature on transition, we refer to [26]. Our own early speculations are presented in [16] and [17].

12.1. **Laminar pipe flow.** We consider the basic case of laminar pipe flow in a pipe directed along the x_1 axis and with cross-section ω, with velocity $u = (u_1, 0, 0)$ and a computed velocity $U = (U_1, 0, 0)$. We assume u and U to depend on (x_2, x_3) and time t, but not on x_1. The associated linearized dual problem (7.1), takes the following form in this case, assuming also the perturbations to be x_1 independent and using that $\bar{U} = (U_2, U_3) = 0$,

$$
\begin{aligned}
-\dot{\varphi}_1 - \nu\Delta\varphi_1 &= 0 \quad && \text{in } \omega \times I,\\
-\dot{\varphi}_2 - \nu\Delta\varphi_2 + \theta_{,2} + U_{1,2}\varphi_1 &= 0 \quad && \text{in } \omega \times I,\\
-\dot{\varphi}_3 - \nu\Delta\varphi_3 + \theta_{,3} + U_{1,3}\varphi_1 &= 0 \quad && \text{in } \omega \times I,\\
\varphi_{2,2} + \varphi_{3,3} &= 0 \quad && \text{in } \omega \times I,\\
\varphi &= 0 \quad && \text{on } \partial\omega \times I,\\
\varphi(\cdot, T) &= \varphi^T \quad && \text{in } \omega,
\end{aligned}
\tag{12.1}
$$

with given initial data φ^T. This problem has a decoupling analogous to that found above for the linearized perturbation equations for parallel flow. In the present dual linearized problem, φ_1 is decoupled from the Stokes-like system for $(\bar{\varphi}, \theta)$, where $\bar{\varphi} = (\varphi_2, \varphi_3)$, with $\varphi_1\bar{\nabla}U_1$ appearing as a driving force. Accordingly, the weak stability factor $S_0(T)$ grows linearly with T or Re, indicating that laminar pipe flow is computable for moderately large Reynolds numbers.

12.2. **An ode-model for transition.** We consider the following initial value problem for a system of two ordinary differential equations: find $w(t) = (w_1(t), w_2(t))$ such that

$$
\begin{aligned}
\dot{w}_1 + \nu w_1 - \lambda w_1 w_2 &= \nu \quad && t > 0,\\
\dot{w}_2 + 2\nu w_2 - \nu w_2 w_1 &= 0 \quad && t > 0,\\
w_1(0) = 1, \quad w_2(0) &= \kappa\nu,
\end{aligned}
\tag{12.2}
$$

where ν is a small positive parameter, and λ and κ are positive parameters of moderate size. The system (12.2) models almost parallel shear flow with w_1 representing the flow velocity in the main direction of the flow, and w_2 the small velocities transversal to the main flow, and the stationary solution $w = (1, 0)$ corresponds to Couette flow between two plates or Poiseuille flow in a pipe. We shall use the model to describe how the small perturbation $\kappa\nu$ of w_2 may cause the base solution $(1, 0)$ to become unstable if $\lambda\kappa$ is larger than some critical value of moderate size.

We shall see that the model (12.2) contains an essential part of the secret of transition to turbulence in parallel flow. The equations for w_1 and w_2 in (12.2) are coupled through the quadratic terms $\lambda w_1 w_2$ and $\nu w_1 w_2$, and model the following selection of terms from the Navier-Stokes equations

$$
\begin{aligned}
\dot{u}_1 - \nu\Delta u_1 + u_{1,2}u_2 &= \nu \quad && t > 0,\\
\dot{u}_2 - \nu\Delta u_2 + u_{2,1}u_1 &= 0 \quad && t > 0,
\end{aligned}
\tag{12.3}
$$

from the momentum equations for the main flow velocity u_1 and the transversal velocity u_2. The nonlinear coupling terms $u_{1,2}u_2$ and $u_{2,1}u_1$ are modeled in the form $\lambda w_1 w_2$ and $\nu w_2 w_1$, corresponding to assuming that $u_{1,2} = -\lambda u_1$ and $u_{2,1} = -\nu u_2$, connecting transversal derivatives of u_1 with u_1 through the parameter λ, and the streamwise derivative of the transversal velocity $u_{2,1}$ with u_2 through the small parameter ν. The relation $u_{2,1} = -\nu u_2$ models a basic feature of parallel flow with the streamwise variations being small. Since we assume initially that $u_2 \approx w_2 \approx \nu$, it corresponds to assuming $u_{2,1} \sim \nu^2$, which is indeed very small. On the other hand, the assumption that $u_{1,2} = -\lambda u_1$ with λ of moderate size corresponds to a natural transversal variation of moderate size of the streamwise velocity in a shear flow.

Note that the coupling term $u_{1,1}u_1$ in the equation for u_1 is not modeled in the form of some multiple of w_1^2. This is because (a) assuming $u_{1,1} \approx \nu^2$, with a corresponding very small term $-\nu^2 w_1^2$ in the model, has no destabilizing effect, and (b) assuming $u_{1,1} = -C\nu$ with a corresponding larger term $-C\nu w_1^2$, which may cause exponential growth through self-resonance in w_1, is not realistic. In fact, (b) is more or less the classical scenario based on the 2d Orr-Sommerfeld equations, which require artificially generated perturbation levels in experiments, for example through heavily vibrating ribbons.

In the transition model, we thus seek to build in realistic features of shear flow including realistic perturbation levels. If we assume zero perturbations, then the model reduces to $\dot{w}_1 + \nu w_1 = 0$, $\dot{w}_2 + 2\nu w_1 = 0$, which has no chance of going unstable. If we assume large perturbation levels, then instability may result immediately. However, none of these scenarios occur in reality, and the role of the model is to explain how small but realistic size perturbations, indeed may cause the initially stable base flow to go unstable after some time. Our model builds the presence of a very small perturbation of order ν^2 of the transversal velocity in the streamwise direction, which naturally may be introduced through the roughness of the pipe. The model does not build on a larger variation of order ν of the streamwise velocity in the streamwise direction, which only seems to be possible with artificially generated perturbations.

The model (12.2) contains the two basic parameters λ and κ, both of moderate size, λ being related to the transversal geometry of the flow such as pipe cross section, $\kappa\nu$ representing a perturbation level in transversal velocities, and $\kappa\nu^2$ a perturbation level in streamwise derivatives of transversal velocities, including both transversal and streamwise perturbations levels. We will see that if $\lambda\kappa$ is larger than some critical value of moderate size, then transition to instability will take place in the model. This indicates that transition in shear flow builds on a combination of features related the transversal geometry and levels of perturbations in both transversal and streamwise direction. We give below computational results for transition in pipe flow supporting this picture.

The system (12.2) has two stationary solutions $w = (1, 0)$ and $w = (2, \nu/(2\lambda))$, with $(1, 0)$ representing the basic Couette or Poiseuille flow. A classical stability analysis based on the eigenvalues of the corresponding linearized system, indicates that $(1, 0)$ is stable and $(2, \nu/(2\lambda))$ is unstable. For example, the linear system obtained linearizing around

$(1,0)$, takes the form

$$\begin{aligned} \dot{\varphi}_1 + \nu\varphi_1 - \lambda_1\varphi_2 &= \nu \qquad t > 0, \\ \dot{\varphi}_2 + \nu\varphi_2 &= 0 \qquad t > 0, \\ \varphi_1(0) = \varphi_{10}, \quad \varphi_2(0) &= \varphi_{20}, \end{aligned} \tag{12.4}$$

where the coefficient matrix $A = [\nu \ -1, 0 \ \nu]$ has a double positive eigenvalue ν. The corresponding coefficient matrix linearizing around $(2, \nu/(2\lambda))$, has one positive (stable) and one negative (unstable) eigenvalue. A classical stability analysis shows that $(1,0)$ is stable under sufficiently small perturbations, and that $(2, \nu/(2\lambda))$ is unstable even under small perturbations. As a result $(1,0)$ is unstable under large perturbations bringing the initial value sufficiently close to the unstable solution $(2, \nu/(2\lambda))$. However, the classical eigenvalue stability analysis is unable to explain the intriguing fact that $(1,0)$ may become unstable even under a small perturbation of the initial data $(1,0)$, if we just have patience to wait! We will now present such a scenario of transition, where the stationary solution $(1,0)$ of (12.2) goes unstable under a small perturbation of initial data of the form $(0, \kappa\nu)$, where κ is a parameter of moderate size, and the scaling with ν makes the perturbation small (since we assume ν to be small). We shall see that if the product $\lambda\kappa$ is above a certain threshold of moderate size, then transition to instability will take place, if we wait over a period of time of length ν^{-1}.

We thus consider the problem (12.2) with the initial data $(1, \kappa\nu)$ close to $(1,0)$, and we ask if the corresponding solution $\bar{w}(t)$ may become unstable after some time. We see that $\dot{\bar{w}}_1(0)/\bar{w}_1(0) = \lambda\kappa\nu$, while $\dot{\bar{w}}_2(0)/\bar{w}_2(0) = -\nu$, which shows that initially $\bar{w}_1$ grows and $\bar{w}_2$ decays at rates $\propto \nu$. Now, $\bar{w}_1$ will continue to grow at that rate as long as $\lambda\bar{w}_2 > \nu$, and further $\bar{w}_2$ will start to grow as soon as $\bar{w}_1 > 2$. Thus, if $\bar{w}_1$ manages to become larger than 2, before $\bar{w}_2$ has decayed below ν/λ, then both components will propel each other in fact a blow up to infinity, corresponding to instability. We shall see that this will occur if $\lambda\kappa$ is above a certain threshold. We notice that the time scale for significant changes in both $\bar{w}_1$ and $\bar{w}_2$ is $\sim \nu^{-1}$, which is a long time since ν is small. The scenario is thus that $\bar{w}_1$ grows slowly at the rate ν over a long time, and if $\lambda\kappa$ is above the threshold, then $\bar{w}_1$ may reach the value 2, where also $\bar{w}_2$ starts to grow after which a blow up follows on a usually somewhat shorter time scale (though still $\propto \nu^{-1}$). This scenario is easy to grasp intuitively, and conforms with the every-day experience of quit sudden blow-up, as a result of an accumulation of small events over a long period.

Solving the linearized equation (12.4) approximately describing the evolution of $\bar{w} - (1,0)$, we find that

$$\bar{w}_1(t) \approx 1 + \varphi_1 = 1 + \lambda\kappa t\nu \exp -t\nu, \quad \bar{w}_2(t) \approx \varphi_2 = \kappa\nu \exp -t\nu, \tag{12.5}$$

which shows the slow growth of $\bar{w}_1$ and slow decay of $\bar{w}_2$ over the long time scale prior to the blow up, occuring if $\lambda\kappa$ is above the threshold. The linear growth in time of φ_1 may be viewed as a consequence of the non-normality of the coefficient matrix A. A classical stability analysis focussing on the double positive eigenvalue ν of $A = [\nu \ -1, 0 \ \nu]$, states that the factor $t \exp -\nu t$ eventually will decay to zero as $t \to \infty$, but misses the substantial transient growth to the level $\propto \nu^{-1}$ after time $\propto \nu^{-1}$ prior to decay. This perturbation

growth of size $\propto \nu^{-1}$ is capable of bringing a solution from the point $(1, \kappa\nu)$ very close to $(1, 0)$, into a neigborhood of the unstable point $(2, \nu(2\lambda))$ with ensuing blow up.

12.3. **Computational transition in Couette and Poiseuille flow.** To verify that the predictions of the model (12.2) applies in the case of nearly parallell flow we present computational results for two test problems: transition to turbulence in Couette and Poiseuille flow in a pipe along the x_1-axis with square cross section 1×1, where we use the cG(1)cG(1) method on a regular tetrahedral mesh with meshsize $h = 1/64$. For both cases we start with a small initial transversal velocity perturbation $\varphi^0 = (0, \varphi_2(x_2, x_3), \varphi_3(x_2, x_3))$ of order 0.1, and we also apply a very small x_1-dependent driving force $f = (0, f_2(x_1), f_3(x_1))$ of order 10^{-3} creating and sustaining a very small streamwise variation of $\bar{u}$, modeling, for example, inperfections in the pipe.

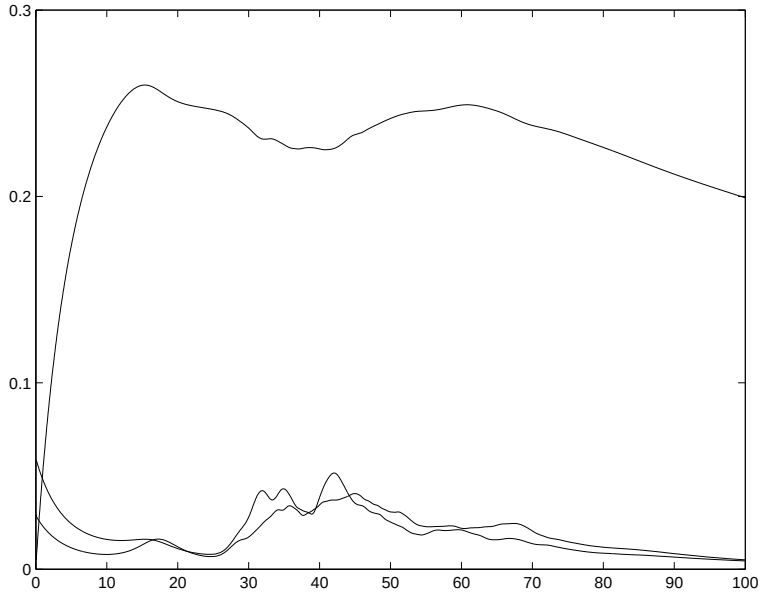

FIGURE 12. Couette flow: $\|\varphi_1\|$, $\|\varphi_2\|$, $\|\varphi_3\|$

The Couette base flow $u = (u_1, 0, 0)$ has a streamwise velocity profile $u_1 = 2x_2 - 1$, with streamwise velocity ± 1 on the top and bottom, slip side walls, and periodic boundary condition in the streamwise direction. Initially, as in the scenario predicted by the model (12.2), the streamwise pertubation φ_1 grows linearly through the action of the Taylor-Görtler mechanism, see Fig.12. In Fig.13 we can see the formation of high velocity streaks due to the Taylor-Görtler mechanism, shifting particles with different streamwise velocities causing the formation of high and low velocity streaks. The pertubations φ_2 and φ_3 decreases initially as predicted by the model (12.2). In the same way, derivatives with respect to x_2 and x_3 grow linearly for u_1, and decreases for u_2 and u_3 (see Fig.14-15). In Fig.16 we see that near $t = 25$ we get a sudden burst where all x_1-derivatives increases by a factor 100 over a short time interval, corresponding to initial transition. We also get

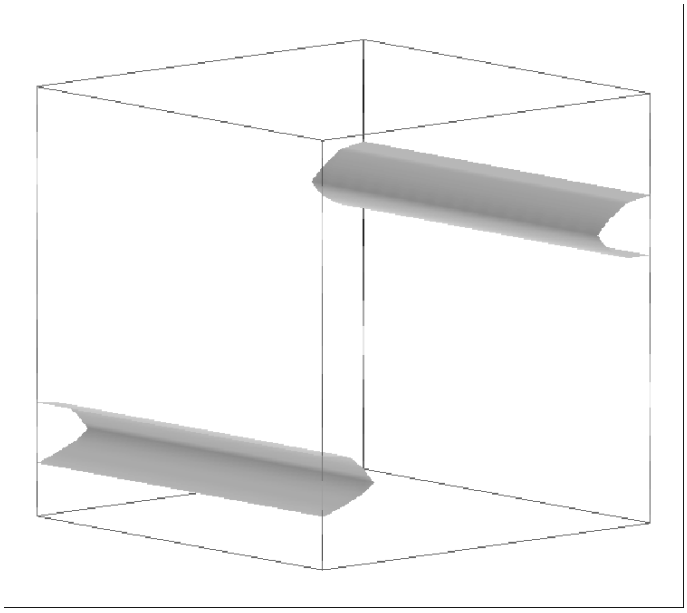

FIGURE 13. Couette flow: Isoconcentration surfaces for φ_1, corresponding to high speed streaks.

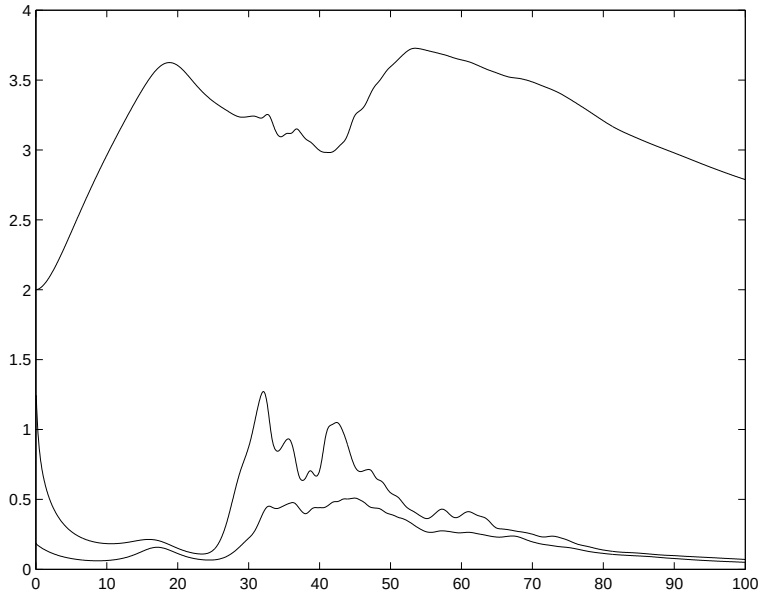

FIGURE 14. Couette flow: $\|du_1/dx_2\|$, $\|du_2/dx_2\|$, $\|du_3/dx_2\|$

a sudden increase in φ_2 and φ_3, see Fig.17, at the same time. A key observation is that the transition is not possible until the pertubation φ_1 and the derivatives $\partial u_1/\partial dx_2$ and $\partial u_1/\partial dx_3$ has reached a certain threshold. Another important observation which is not obvious from studying the global norms is that the pertubations of course vary in space

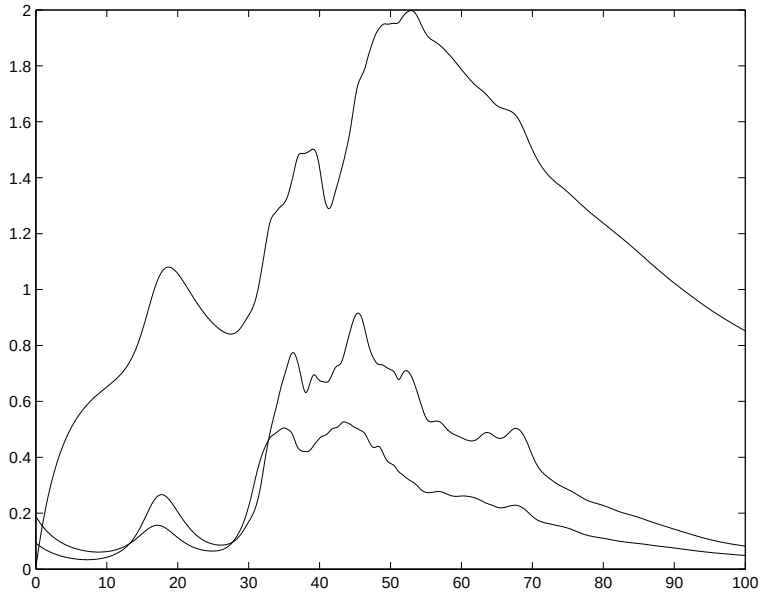

FIGURE 15. Couette flow: $\|du_1/dx_3\|$, $\|du_2/dx_3\|$, $\|du_3/dx_3\|$

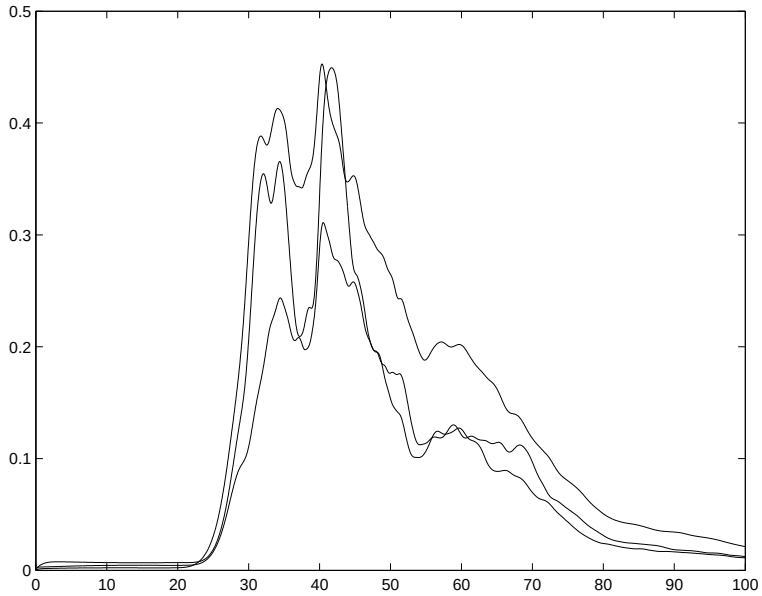

FIGURE 16. Couette flow: $\|du_1/dx_1\|$, $\|du_2/dx_1\|$, $\|du_3/dx_1\|$

and that the threshold is a local condition that have to be satisfied. In Fig.18 we can follow the initial phase of the transition.

The Poiseuille base flow has a streamwise velocity profile $u_1(x_2, x_3) = 16y(1-y)z(1-z)$ in a channel with no slip walls and a force term $f = (32(y(1-y)+z(1-z)), 0, 0)$, where we

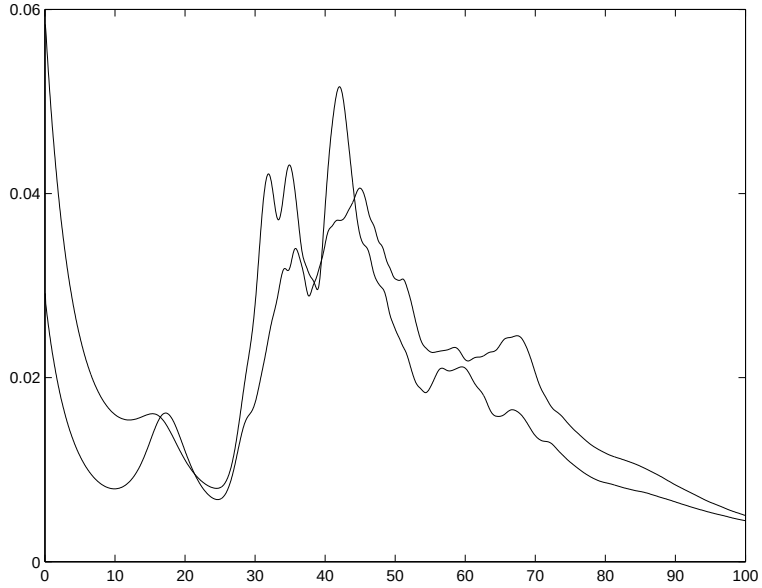

FIGURE 17. Couette flow: $\|\varphi_2\|$, $\|\varphi_3\|$

use periodic boundary conditions in the streamwise direction. In Fig 19 we show the perturbation growth in the L_2-norm and note a linear growth in the streamwise pertubation corresponding to the Taylor-Görtler mechanism, whose action is shown in Fig 21 slowly shifting particles with different streamwise velocity transversally with a considerable reorganization of the streamwise velocity from the transversal perturbation. Fig.20 shows the L_2-norm of the x_1-derivatives in the solution as a function of time, with a sudden increase near $t = 6$. Again we note that this increase is not possible until the x_1-pertubation φ_1 is large enough.

We note that while the computations are valid in the initial phase of the transition, the computational mesh is too coarse for an accurate *direct numerical simulation* (DNS) of turbulent flows following the transition. To be able to compute turbulent flows we either need a very fine mesh, resolving the finest scales in the flow, or a turbulence model of some sort, which is the topic of the next section.

13. TURBULENCE MODELING: DLES

We now turn to the topic of turbulence modeling. There are many different approaches to this problem, for an overview we refer to [6]. Here we are going to consider the case of *Large Eddy Simulations* (LES), where we compute the larger scales of motion in the flow and model the effect of the finer unresolved scales in a so called subgrid model. The basic problem is to model the divergence of the Reynolds stress tensor $(\tau_{ij}(u))$ with components

$$\tau_{ij}(u) = (u_i u_j)^h - u_i^h u_j^h,$$

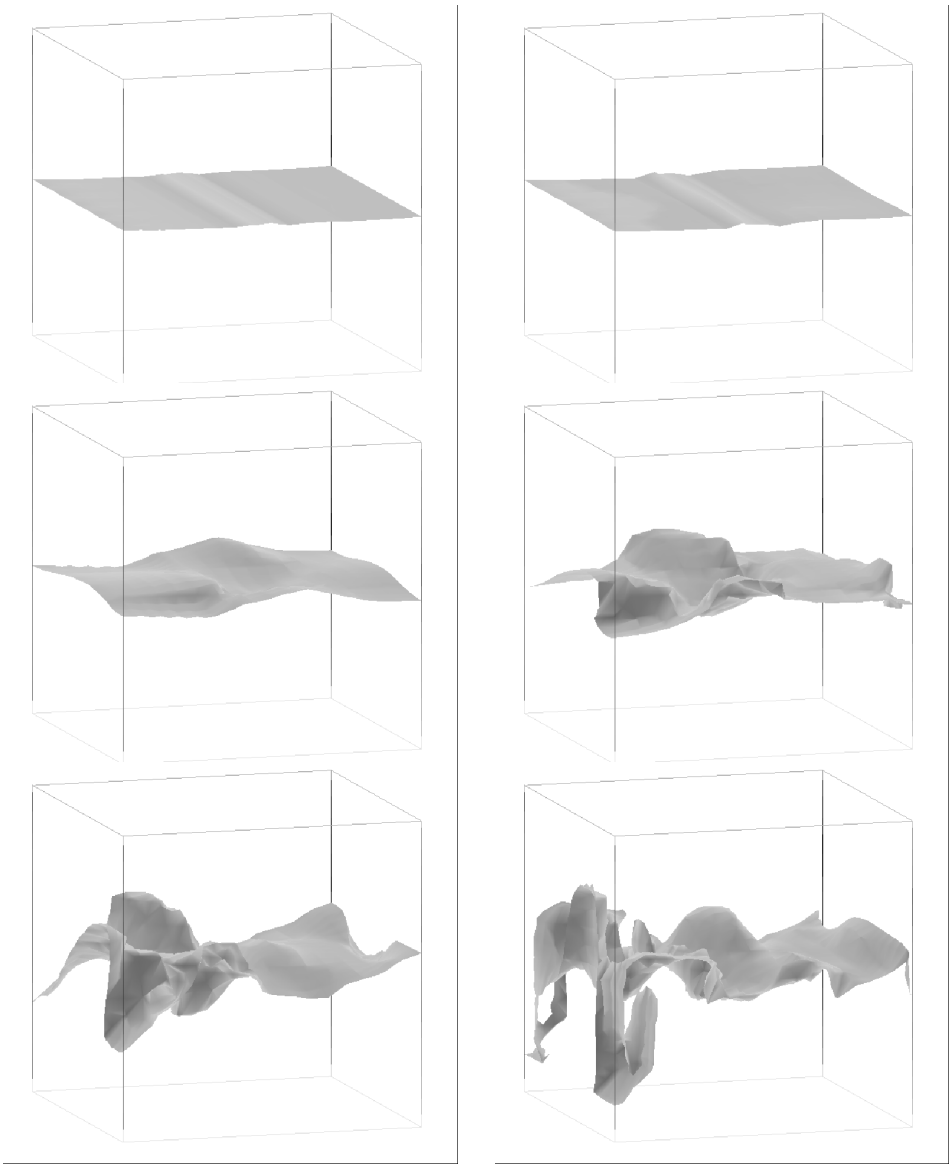

FIGURE 18. Streamwise velocity zero isosurfaces in Couette flow for $t = 20, 25, 30, 32, 34, 40$, showing the initial phase of the transistion

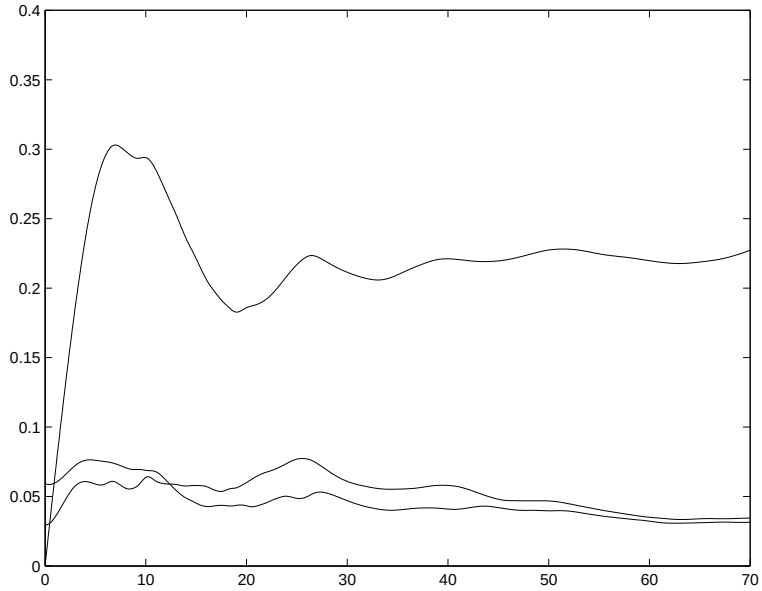

FIGURE 19. Poiseuille flow: $\|\varphi_1\|$, $\|\varphi_2\|$, $\|\varphi_3\|$

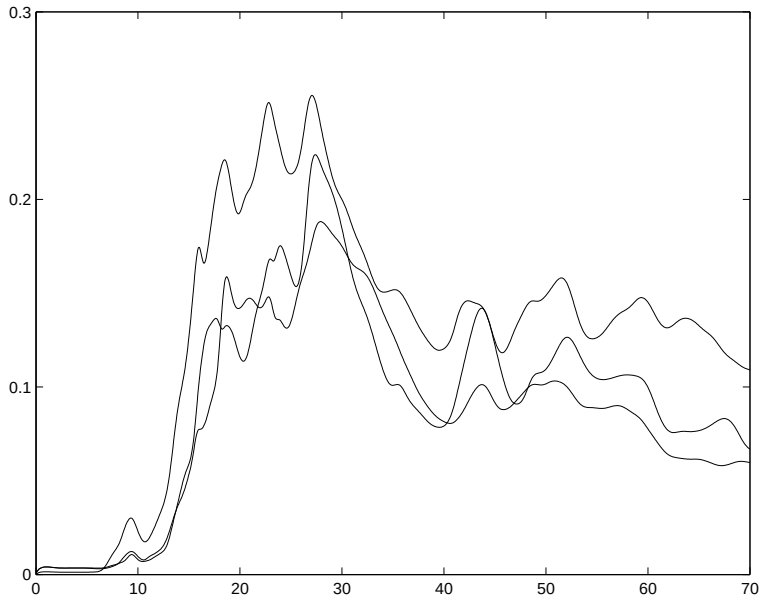

FIGURE 20. Poiseuille flow: $\|du_1/dx_1\|$, $\|du_2/dx_1\|$, $\|du_3/dx_1\|$

where v^h represents a local running average of v in space of size h, in terms of u^h. The classical turbulent viscosity model is the *Smagorinsky model* with the components of τ_{ij}

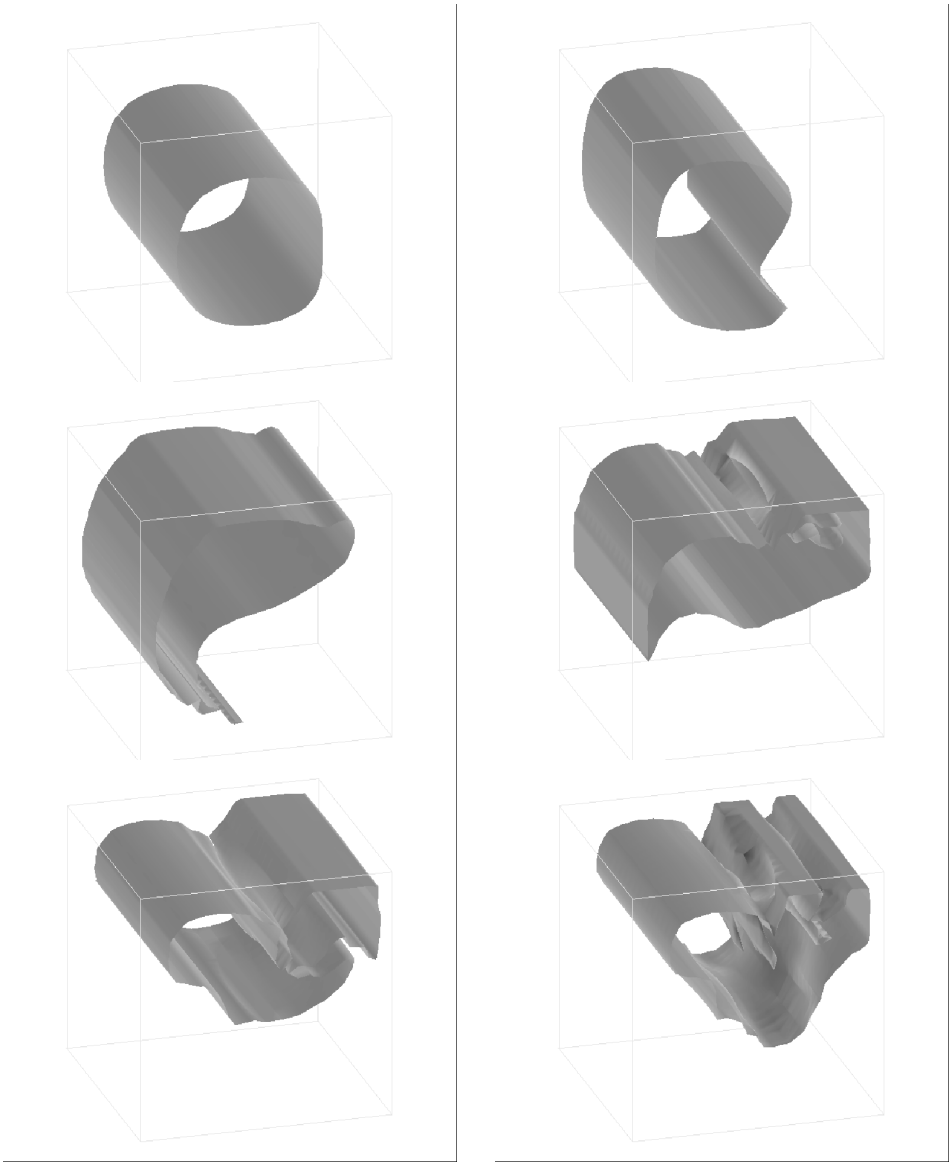

FIGURE 21. Streamwise velocity isosurfaces in Poiseuille flow at $t = 1, 3, ..., 15$, illustrating the Taylor-Görtler mechanism

given by

$$\tau_{ij} - \frac{1}{3}\tau_{kk} = -2\nu_T \epsilon_{ij}(u^h),$$

with

$$\nu_T = (C_S h)^2 |\epsilon(u^h)|$$

where C_S is the Smagorinsky constant.

In general, the resolved scales in a LES are assumed to lie in the so called inertial range (see [6]), which refers to a range of scales for which the energy spektrum has a simple power law behaviour, corresponding to scale similarity. Different types of scale similarity assumptions also on the Reynolds stresses have been used to motivate various types of subgrid models. For example, in *Dynamic Large eddy Simulation* (DLES) [8] the parameters in a particular model are determined by comparing resolved Reynolds stresses on different scales. In scale similarity models [24] the assumption is that the exact Reynolds stresses are proportional to the resolved Reynolds stresses.

In [10, 11, 12, 13] we used an assumption based on the existence of a scale similarity with respect to a *Haar Multiresolution Analysis* (MRA) generated by the hierarchy of successively refined computational meshes. Scale similarity with respect to a Haar MRA has been observed, for example, in experimental aerothermal data [22]. We will base a subgrid model on an Ansatz of the form

$$\tau_{ij}(x,t) \approx C(x,t) h^{\mu(x,t)} \tag{13.1}$$

with the coefficients $C(x,t)$ and $\mu(x,t)$ to be found by fitting the model on coarser scales.

We first discuss a similar subgrid modeling problem for reaction-convection-diffusion problems and present results based on scale similarity. We then discuss results from computation and experiments indicating that turbulent flow has some scale similarity features and thus may be open to the same approach.

13.1. **Subgrid modeling in reaction-diffusion-convection problems.** In recent years methods of *dynamic subgrid modeling* have been proposed, in particular in turbulence modeling in DLES by Germano (1991). The purpose of a subgrid model is to model the effect of unresolvable scales on resolvable scales corresponding to closure in turbulence modeling. The basic idea in dynamic subgrid modeling is to fit a particular subgrid model based on computed solutions on different resolvable scales, and then extrapolate the model to subgrid scales. In order for such a process based on scale extrapolation to work, it is necessary that the underlying problem has some 'scale similarity', so that the experience gained by fitting the model on a coarse scale with a fine scale solution as reference may be extrapolated to the finer scale. It is conceivable that many problems involving a range of scales from large to small, such as fluid flow at larger Reynolds numbers and flow in heterogeneous porous media, in fact do have such a scale similarity, once the larger scales related to the geometry of the particular problem have been resolved.

In [10] we initiated a study of dynamic subgrid modeling in a stationary convection-diffusion problem with fractal coefficients, where a subgrid model in the form of a corrective force is extrapolated from coarser grids with the finest computational grid as reference. We

showed that the quality of the solution on mesh size h with extrapolated subgrid model, is comparable to that of a solution without subgrid model on a scale $h/4$ or smaller. We here present extensions to time-dependent convection-diffusion-reaction systems with 'fractal' solutions, where the fractality again originates from data (see [10, 11, 12]). The relevance of studying fractal models is motivated by the abundant number of experimental observations of fractality in turbulent flows, see e.g. [25] and references therein. Extensions to Navier-Stokes equations with the goal of connecting with DLES is under way.

In the setting of a general problem of the form $A(u) = f$ of Section 1.6 with exact solution u, the problem of subgrid modeling can be formulated as follows: For a given function v, let v^h represent a local average on a scale h which represents the finest computational scale. We seek an equation for the average u^h of the exact solution u and by averaging the equation $A(u) = f$ and we obtain $A(u^h) + F_h(u) = f^h$, where $F_h(u) \equiv (A(u))^h - A(u^h)$ has to be modeled in terms of u^h to get a modified equation $\hat{A}(\hat{u}) = A(\hat{u}) + \hat{F}_h(\hat{u}) = f^h = \hat{f}$, where the function $\hat{F}_h$ is the subgrid model and $\hat{F}_h(\hat{u})$is supposed to approximate $F_h(u)$. In dynamic subgrid modelling we seek to model $F_h(u)$ by extrapolation from computing $F_H(U_h)$ where $H > h$ and U_h is a computed solution on the scale h.

13.2. **Systems of convection-diffusion-reaction equations.** We consider a model problem of the form: Find $u : \Omega \times [0,T] \to R^n$ such that

$$\dot{u} + Lu = \dot{u} - \epsilon\Delta u + \beta \cdot \nabla u = f(u), \quad \forall (x,t) \in \Omega \times (0,T), \tag{13.2}$$

$$u = u_D, \quad \forall (x,t) \in \Gamma_D \times (0,T), \quad \frac{\partial u}{\partial n} = u_N, \quad \forall (x,t) \in \Gamma_N \times (0,T), \tag{13.3}$$

$$u(x,0) = u_0(x), \quad \forall x \in \Omega, \tag{13.4}$$

where $f : R^n \to R^n$ is smooth, $\Omega \subset R^d$ and $\partial\Omega = \Gamma_D \bigcup \Gamma_N$. Typically we will assume that ϵ is small and that the solution u to (13.2)–(13.4) contains a range of scales, from very small scales to large scales, induced either by the initial condition $u_0(x)$ or by the differential operator L through β. Assuming we want to find an approximation of u on the scale h, representing the finest spatial computational scale, we define for each fixed t the spatial *running average* u^h of u on the scale h by

$$u^h(x,t) = \frac{1}{h^d} \int_{x_1-h/2}^{x_1+h/2} ... \int_{x_d-h/2}^{x_d+h/2} u(y,t)\ dy_1...dy_d, \tag{13.5}$$

where we note that this operator commutes with space and time differentiation. Applying this operator to (13.2)–(13.4) we find that the running average u^h satisfies the following equation (modulo boundary effects)

$$\dot{u}^h + L_h u^h = \dot{u}^h + \beta^h \cdot \nabla u^h - \epsilon\Delta u^h = f(u^h) + F_h(u), \quad u^h(x,0) = u_0^h(x), \tag{13.6}$$

where L_h is a simplified operator on the scale h resulting from approximating β by β^h and the correction term $F_h(u) = (f(u))^h - f(u^h) + L_h u^h - (Lu)^h$ contains the influence of the unresolved scales on u^h. We consider a computational problem without subgrid model of the form

$$\dot{u}_h + L_h u_h = f(u_h), \quad u_h(x,0) = u_0^h(x), \tag{13.7}$$

and a corresponding problem with subgrid model of the form

$$\dot{\hat{u}}_h + L_h\hat{u}_h = f(\hat{u}_h) + \hat{F}_h(\hat{u}_h), \quad \hat{u}_h(x,0) = u_0^h(x), \tag{13.8}$$

where $\hat{F}_h(\hat{u}_h)$ should approximate $F_h(u)$. In this note we will consider a subgrid model of the form $\hat{F}_h(\hat{u}_h) = g(F_h(\hat{u}_h), F_{2h}(\hat{u}_h), F_{4h}(\hat{u}_h))$ based on averaging on the coarser scales $2h$ and $4h$, where the function g is derived based on a scale regularity assumption on $F_h(u)$.

13.3. **Analysis of $F_h(u)$ using the Haar MRA.** In the rest of this section we let $\Omega = [0,1]^2$ and for each $h = 2^{-i}$, with $i = 0, 1, ...$, we define a corresponding regular quadratic mesh τ^h with elements corresponding to subdomains $\Omega_{i,k}$ with side length h. We denote the space of piecewise constant functions on τ^h by V_i, and the closure of the union of the V_j's is equal to $L_2(\Omega)$. The chain of closed subspaces $V_0 \subset V_1 \subset ... \subset V_j \subset ...$ is denoted a Haar Multi-resolution Analysis of $L_2(\Omega)$.

Each V_j is spanned by the dilates and integer translates of one *scale function* $\Phi \in V_0$, that is, $V_j = \text{span}\{\Phi_{j,k}(x) = 2^j\Phi(2^jx - k)\}$. The functions $\Phi_{j,k}$ form an L_2-orthonormal basis in V_j, and we denote the orthogonal complement of V_j in V_{j+1} by W_j, which is generated by another orthonormal basis (the *wavelets*) $\Psi_{j,k}(x) = 2^j\Psi(2^jx - k)$, where $\Psi \in W_0$ is called the *mother wavelet*. $W_j = W_j^1 \oplus W_j^2 \oplus W_j^3$, where the W_j^ν's represent differences in the horizontal, vertical and diagonal directions respectively. The space $L_2(\Omega)$ can now be represented as the direct sum $L_2(\Omega) = V_0 \oplus W_0^1 \oplus ... \oplus W_0^3 \oplus ... \oplus W_j^1 \oplus ... \oplus W_j^3 \oplus ...$, and each $f \in L_2(\Omega)$ has a unique decomposition $f = f_\Phi\Phi + \sum_{j,k} f_{j,k}^1\Psi_{j,k}^1 + ... + f_{j,k}^3\Psi_{j,k}^3 = f_\Phi + \sum_j f_j^1 + ... + f_j^3$, where the f_j^ν's represent the contributions on the different scales 2^{-j}. For the one dimensional Haar MRA in $L_2([0,1])$, the scale function is defined by $\varphi(x) = 1$ for $x \in [0,1]$ and 0 else, and the mother wavelet is defined by $\psi(x) = 1$ for $x \in (0, 1/2)$, -1 for $x \in (1/2, 1)$ and 0 else. In two dimensions the scale function and the wavelets are tensor products of the one dimensional scale function and wavelets. For the two dimensional Haar MRA in $L_2(\Omega)$ we have the scale function $\Phi(x_1, x_2) = \varphi(x_1)\varphi(x_2)$ and the wavelets $\Psi^1(x_1, x_2) = \varphi(x_1)\psi(x_2)$, $\Psi^2(x_1, x_2) = \psi(x_1)\varphi(x_2)$, $\Psi^3(x_1, x_2) = \psi(x_1)\psi(x_2)$. For $f \in L_2(\Omega)$, we define $[f]^h = f_\varphi + \sum_{j<i} f_{j,k}^1\Psi_{j,k}^1 + f_{j,k}^2\Psi_{j,k}^2 + f_{j,k}^3\Psi_{j,k}^3$. The linear mapping $L_2 \ni f \to [f]^h \in V_i$ can then be identified with the L_2-projection of f onto V_i, and we note that $[f]^h = \bar{f}^h$, where $\bar{f}^h$ is the piecewise constant function on τ^h that equals f^h in the midpoints of each element in τ^h. If we let $\bar{F}_h(u)$ denote the piecewise constant function on τ^h that equals $F_h(u)$ in the midpoints of the elements of τ^h, we have

$$\bar{F}_h(u) = [f(u)]^h - f([u]^h) - ([\beta \cdot \nabla u]^h - [\beta]^h \cdot [\nabla u]^h),$$

which for second order reaction terms $f(u)$ leads us to model covariances of the form

$$E_h(v, w) = [vw]^h - [v]^h[w]^h, \tag{13.9}$$

for given functions v and w. The following observation from [11] shows that $E_h(v, w)$ equals the sum of the Haar coefficients corresponding to scales finer than and equal h, scaled by

the area of the elements in τ^h: if $x \in \Omega_{i,k}$ then

$$E_h(v,w)(x) = 2^{2i} \sum_{\substack{j \geq i \\ l\,:\,\Omega_{j,l} \subset \Omega_{i,k}}} (v^1_{j,l} w^1_{j,l} + v^2_{j,l} w^2_{j,l} + v^3_{j,l} w^3_{j,l}). \tag{13.10}$$

13.4. **Scale extrapolation using self-similarity.** We base our subgrid model on an Ansatz of the form of each separate covariance

$$E_h(v,w)(x) \approx C(x) h^{\mu(x)}, \quad x \in \Omega, \tag{13.11}$$

with the coefficients $C(x)$ and $\mu(x)$ to be extrapolated. The Ansatz can be motivated from (13.10) assuming scale similarity of the Haar coefficients corresponding to fractality. The Ansatz leads to the following extrapolation formula: $\hat{F}_h(\hat{u}_h) = \sum \hat{E}_h(\hat{v}_h, \hat{w}_h)$, where

$$\hat{E}_h(\hat{v}_h, \hat{w}_h) = g(E_h(\hat{v}_h, \hat{w}_h), E_{2h}(\hat{v}_h, \hat{w}_h), E_{4h}(\hat{v}_h, \hat{w}_h)) \tag{13.12}$$

with

$$g(a,b,c) = (1 - (\frac{c - b^{4h}}{b^{4h} - a^{4h}})^{-n}) \frac{b^{4h} - a^{4h}}{\frac{c - b^{4h}}{b^{4h} - a^{4h}} - 1} \tag{13.13}$$

and $2^{-(n+i)}$ is the finest scale present in the exact solution.

13.5. **Applications.** In all examples we will have $h = 2^{-5}$. We construct two dimensional fractal data as sums of local tensor products of the one dimensional fractal *Weierstrass function* $W_{\gamma,\delta}(x) = \gamma \sum_{j=0}^{N} 2^{-j\delta} \sin(2^j \cdot 2\pi x)$, where we let $\gamma = \delta = 0.1$ in all examples.

13.5.1. *Volterra-Lotka (VL).* We consider a reaction dominated problem of the form

$$\dot{u}_1 - \epsilon \Delta u_1 = u_1(1 - u_2), \quad \dot{u}_2 - \epsilon \Delta u_2 + \beta \cdot \nabla u_2 = u_2(u_1 - 1),$$
$$\frac{\partial u}{\partial n}|_{\partial\Omega} = 0, \quad u(x,0) = (W^{2D}_{\gamma,\delta}(x), 1),$$

where $\epsilon = 10^{-6}$, which corresponds to the classical Volterra-Lotka system with small diffusion and convection in one component. We have $F_h(u) = (-(u_1 u_2)^h + u_1^h u_2^h, (u_1 u_2)^h - u_1^h u_2^h)$, and with subgrid model we have that $\hat{F}_h(\hat{u}_h) = (-\hat{E}_h(\hat{u}_1, \hat{u}_2), \hat{E}_h(\hat{u}_1, \hat{u}_2))$, with $n = 4$ (the 2-logarithm of the reference scale minus the computational scale). For these problems we use a central difference-Crank-Nicolson scheme for the midpoints of the elements, where we let these midpoint values represent a piecewise constant approximation over the elements, and the reference scale is 2^{-9} in the computation of the error. The solutions are oscillating and both u_1 and u_2 are fractal for $t > 0$, even though $u_2(x,0) = 1$. We want to approximate u^h, and the errors $\|u^h - U_h\|$ are shown in Tab.7-9, where U_h is the solution without model, without model but computed on the finer scale $h/2$ and then projected onto the scale h, with the subgrid model (13.13), and with a simplified model $\hat{F}_h(\hat{u}_h) = F_{2h}(\hat{u}_h, \hat{u}_h)$ corresponding to a standard scale similarity model. We first let $\beta = 0$ and compute to $T = 2$, then we let β be a rotational mixing of order h: $\beta = h\ (\sin(\pi x_1)\cos(\pi x_2), -\cos(\pi x_1)\sin(\pi x_2))$ and here we only compute to $T = 1$, since after $T = 1$ the subgrid scales are dominated by the

TABLE 7. Error in $u_1$in L_1-norm for VL with $\beta = 0$

subgrid model	$t = 0.5$	$t = 1.0$	$t = 1.5$	$t = 2.0$
no model	$1.9{\cdot}10^{-3}$	$7.2{\cdot}10^{-3}$	$1.1{\cdot}10^{-2}$	$1.1{\cdot}10^{-2}$
no model on $h/2$	$1.4{\cdot}10^{-3}$	$4.6{\cdot}10^{-3}$	$7.0{\cdot}10^{-3}$	$6.8{\cdot}10^{-3}$
$\tilde{F}_h(\tilde{u}_h) = F_{2h}(\tilde{u}_h, \tilde{u}_h)$	$1.4{\cdot}10^{-3}$	$4.8{\cdot}10^{-3}$	$6.5{\cdot}10^{-3}$	$6.3{\cdot}10^{-3}$
formula (13.13)	$1.0{\cdot}10^{-3}$	$2.8{\cdot}10^{-3}$	$3.8{\cdot}10^{-3}$	$4.2{\cdot}10^{-3}$

TABLE 8. Error in $u_2$in L_1-norm for VL with $\beta = 0$

subgrid model	$t = 0.5$	$t = 1.0$	$t = 1.5$	$t = 2.0$
no model	$1.4{\cdot}10^{-4}$	$3.4{\cdot}10^{-4}$	$2.0{\cdot}10^{-4}$	$4.4{\cdot}10^{-4}$
no model on $h/2$	$1.0{\cdot}10^{-4}$	$2.1{\cdot}10^{-4}$	$1.2{\cdot}10^{-4}$	$2.9{\cdot}10^{-4}$
$\tilde{F}_h(\tilde{u}_h) = F_{2h}(\tilde{u}_h, \tilde{u}_h)$	$9.0{\cdot}10^{-5}$	$2.0{\cdot}10^{-4}$	$1.5{\cdot}10^{-4}$	$2.8{\cdot}10^{-4}$
formula (13.13)	$7.0{\cdot}10^{-5}$	$1.4{\cdot}10^{-4}$	$1.5{\cdot}10^{-4}$	$2.4{\cdot}10^{-4}$

TABLE 9. Error in $u_1$in L_1-norm for VL with $\beta \neq 0$

subgrid model	$t = 0.5$	$t = 1.0$	$t = 1.5$	$t = 2.0$
no model	$2.5{\cdot}10^{-5}$	$1.5{\cdot}10^{-4}$	$3.4{\cdot}10^{-4}$	$6.4{\cdot}10^{-4}$
no model on $h/2$	$2.5{\cdot}10^{-5}$	$1.1{\cdot}10^{-4}$	$1.9{\cdot}10^{-4}$	$3.3{\cdot}10^{-4}$
$\tilde{F}_h(\tilde{u}_h) = F_{2h}(\tilde{u}_h, \tilde{u}_h)$	$2.5{\cdot}10^{-5}$	$1.1{\cdot}10^{-4}$	$2.1{\cdot}10^{-4}$	$5.0{\cdot}10^{-4}$
formula (13.13)	$2.0{\cdot}10^{-5}$	$6.0{\cdot}10^{-5}$	$2.0{\cdot}10^{-4}$	$5.6{\cdot}10^{-4}$

convective streaks due to β. We study the error for each component individually, and for $\beta = 0$ we find that the solution with the subgrid model is the best for both components, even though the modeling errors are smaller in u_2 since $u_2(x, 0)$ is constant. For $\beta \neq 0$ the solution with the subgrid model is best for u_1 but, because of the convection, subgrid scales in u_2 do not develop and the solutions with subgrid models does not differ significantly from the solution without subgrid model. The solution on $h/2$ is better since the discretization error is then reduced.

13.5.2. *Fractal convection (FC).* We now consider a convection dominated problem of the form

$$\dot{u} + \beta \cdot \nabla u - \epsilon \Delta u = 1, \quad u|_{x_1=0,x_2=0} = 0, \quad \frac{\partial u}{\partial n}|_{x_1=1,x_2=1} = 0, \quad u(x, 0) = 0, \tag{13.14}$$

TABLE 10. Error in L_1-norm for FC

subgrid model	$t = 0.25$	$t = 0.5$	$t = 0.75$	$t = 1.0$
no model	$7.2{\cdot}10^{-3}$	$1.2{\cdot}10^{-2}$	$1.1{\cdot}10^{-2}$	$1.1{\cdot}10^{-2}$
formula (13.13)	$5.8{\cdot}10^{-3}$	$7.2{\cdot}10^{-3}$	$6.2{\cdot}10^{-3}$	$6.2{\cdot}10^{-3}$

for $\beta = (W^{2D}_{\gamma,\delta}, W^{2D}_{\gamma,\delta})$ and $\epsilon = 10^{-3}$, which we solve by a Streamline Diffusion cG(1)cG(1) method [2] with bilinear, quadratic elements. In the computation of the error the reference scale is 2^{-8}. The solution is in this case relatively smooth since the fractal field β is now only acting on the derivatives of the solution. We have that $F_h(u) = \beta^h \cdot (\nabla u)^h - (\beta \cdot \nabla u)^h$, and the error in the solution with the subgrid model is smaller than in the solution without subgrid model.

13.6. **Do we have scale similarity in turbulent flows?** The above discussion is based on an assumption of scale similarity of covariances of individual solution components, with respect to the Haar basis induced by a mesh hierarchy. In 3d we get a corresponding Haar basis induced by the tetrahedral mesh hierarchy used in the above computations of transition to turbulence, see Fig.22. In Fig.23 we have plotted the sum of Haar coefficients on three different scales, of the Reynolds stress component τ^{8h}_{11} ($h = 1/64$) for the Couette flow from Section 12.3 at $t = 30$, which has started its transition to turbulence but is not fully developed (the component τ_{11} is chosen since the streamwise velocity dominates the Couette flow). The plot shows 60 elements in the coarsest mesh corresponding to the scale $8h$, and we see that the decrease in the Haar coefficients is reasonable regular and we consider this as some evidence of scale similarity of the Reynolds stresses for this flow, although this test is not satisfactory because the turbulence is not fully developed and the computational mesh is too coarse to represent a fully developed turbulent flow. For experimental observations of fractality in turbulent flows we refer to e.g. [22] or [25] and references therein.

13.7. **A posteriori error estimation for turbulent flow.** In deriving a posteriori error estimates for turbulent flows we have to take into account both the numerical error from discretization and the modeling error from subgrid modeling. We explain the basic steps in the setting of a general subgrid modeling problem $A(u) = f$, where u is the exact solution. Due to subgrid scales in u we can not compute a pointwise accurate approximation to u. Instead we aim for a pointwise accurate approximation of u^h, where u^h represent a local average of u on a scale h, which represents the finest computational scale. We seek an equation for the average u^h of the exact solution u and by averaging the equation $A(u) = f$ we obtain $A(u^h) + F_h(u) = f^h$, where $F_h(u) \equiv (A(u))^h - A(u^h)$ has to be modeled in terms of u^h to get a modified equation $\hat{A}(\hat{u}) = A(\hat{u}) + \hat{F}_h(\hat{u}) = f^h = \hat{f}$, where $\hat{u}$ is an approximation of u^h and $\hat{F}_h(\hat{u}) \approx F_h(u)$ represents a subgrid model.

We then solve the Galerkin equation: find $U_h \in V_h$ such that $(A(U_h) + \hat{F}_h(U_h), v) = f^h$, for all $v \in V_h$, where V_h is a finite dimensional subspace, on a mesh of size h, of the Hilbert

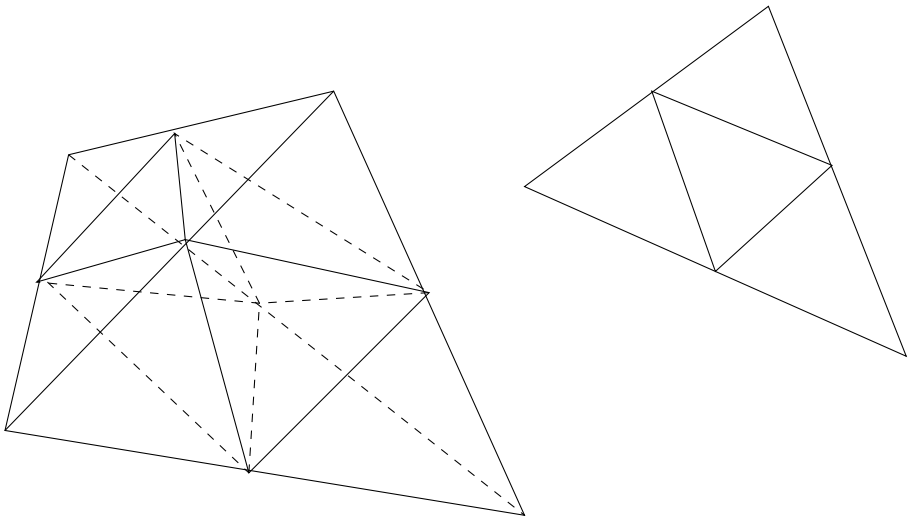

FIGURE 22. Haar MRA generated from successively refining unstructured tetrahedral and triangular meshes, in 3d and 2d respectively.

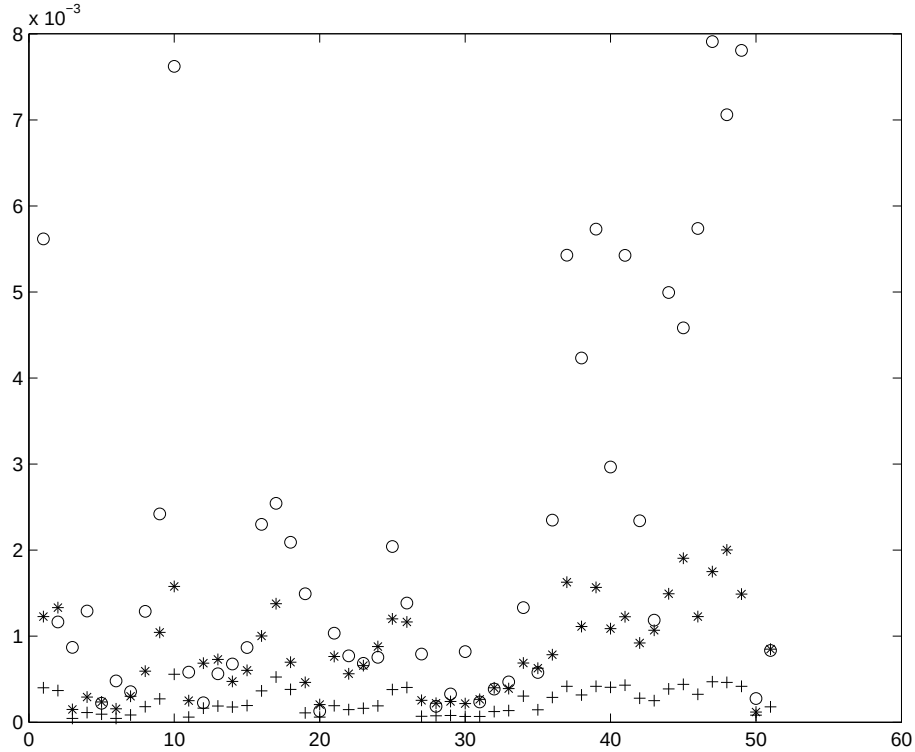

FIGURE 23. Couettte flow at $t = 21$: sum of Haar coefficients for $\tau_{11}^{8h}(U_h)$ on scales $8h$ ($'o'$), $4h$ ($'*'$), and $2h$ ($'+'$)

space V with inner product $(\cdot,\cdot)$ and norm $\|\cdot\|$. U_h is now an approximation of u^h and the error $e = u^h - U_h$ is therefore the appropriate error to study, not $u - U_h$. This means that the appropriate linearized dual problem to solve is $(A'(u^h, U_h)w, \varphi) = (w, \psi)$, for all $w \in V$, where $A'(u^h, U_h)e = A(u^h) - A(U_h)$, that is we linearize the dual problem at u^h and not at the exact solution u. When we solve the dual problem numerically we do not have access to u^h and we will therefore have to use U_h instead of u^h. The linearization error is then $u^h - U_h$, which we anticipate to be pointwise small. If we on the other hand linearize at the exact solution u we get a linearization error $u - U_h$, which is not pointwise small. We get the following error representation

$$\begin{aligned}(e,\psi) &= (u^h - U_h, \psi) = (A'(\hat{u}^h, U_h)e, \varphi) = (A(u^h) - A(U_h), \varphi)\\ &= (f^h - F_h(u) - A(U_h), \varphi) = (f^h - A(U_h) - \hat{F}_h(U_h), \varphi)\\ &+ (\hat{F}_h(U_h) - F_h(u), \varphi) = (\hat{R}(U_h), \varphi) + (\hat{F}_h(U_h) - F_h(u), \varphi),\end{aligned}$$

where $R(U_h) = f^h - A(U_h) - \hat{F}_h(U_h)$ is a computable numerical residual related to the discretization error in solving the equation $A(\hat{u}) + \hat{F}_h(\hat{u}) = f^h$, and $\hat{F}_h(U_h) - F_h(u)$ is a modeling residual related to the error in the subgrid model $\hat{F}_h$. We note that the linearized dual problem is independent of both $F_h(u)$ and $\hat{F}_h$, and thus contain the stability properties of the average u^h.

Even if we do not use a turbulence model in computing U_h we will have to estimate $F_h(u)$, possibly by using a turbulence model. Using a turbulence model $\hat{F}_h$ in computing U_h, we instead need to estimate $F_h(u) - \hat{F}(U_h)$.

14. Multi-adaptivity: individual time-steps

We finally present the multi-adaptive Galerkin methods mcG(q) and mdG(q) with individual time steps for different solution components developed in [21]. We consider an initial value problem of the form

$$\begin{aligned}u_t + f(t,u) &= 0 \qquad \text{for } 0 < t < T,\\ u(0) &= u_0,\end{aligned} \tag{14.1}$$

where $f(t,\cdot) : \mathbb{R}^N \to \mathbb{R}^N$ is a given mapping, $u_t = \frac{du}{dt}$, and T is a final time. To formulate the mcG(q)-method, we partition the interval $(0,T)$ individually for the different components with individual time-intervals $\{I_{ij}\}_j$ and time-steps $\{k_{ij}\}_j$ for every individual component $U_i(t)$. The mcG(q)-method for (14.1) reads: Find $U \in V$ with $U(0) = u_0$, such that

$$\int_0^T (\dot{U}, v)\, dt + \int_0^T (f(U,\cdot), v)\, dt = 0 \;\forall v \in W,$$

where

$$\begin{aligned}V &= \{v \in C([0,T]) : v_i|_{I_{ij}} \in \mathcal{P}^{q_{ij}}(I_{ij}),\ j = 1,\ldots,M_i,\ i = 1,\ldots,N\},\\ W &= \{v : v_i|_{I_{ij}} \in \mathcal{P}^{q_{ij}-1}(I_{ij}),\ j = 1,\ldots,M_i,\ i = 1,\ldots,N\},\end{aligned}$$

and where $\mathcal{P}^q(I)$ denotes the linear space of polynomials of degree $\leq q$ on I. The trial functions in V are thus continuous piecewise polynomials, locally of degree q_{ij}, and the

test functions in W are discontinuous piecewise polynomials that are locally of degree $q_{ij}-1$. The mdG(q) method is similar with discontinuous trial functions of degree q_{ij} and discontinuous test functions also of degree q_{ij}.

14.1. **Computability and predictability of the Solar System.** We consider the problem of computability and predictability of the Solar System, with the objective of using a multi-adaptive solver with individual time steps for individual components, see [21] where also applications to heat flow and the Burgers equation are presented. We expect multi-adaptivity to be of importance also in CFD.

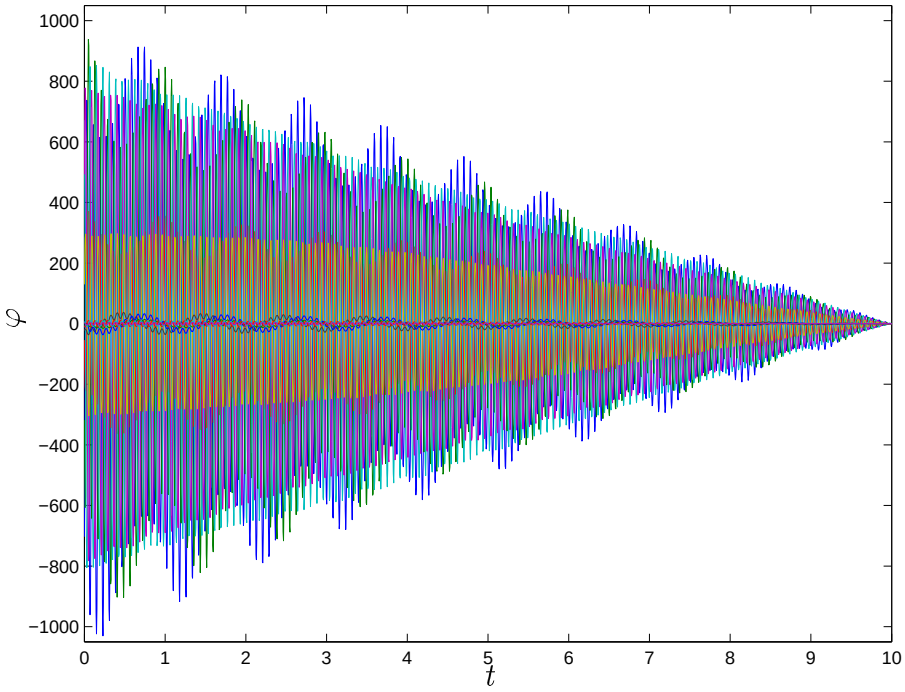

FIGURE 24. Part of the dual of the Solar System with data chosen for control of the error in position of the Moon at final time.

We thus consider the Solar System, including the Sun, the Moon, and the nine planets, which is a particular n-body problem of fundamental importance:

$$m_i\ddot{x}_i = \sum_{j\neq i} \frac{Gm_im_j}{|x_j - x_i|^3}(x_j - x_i), \tag{14.2}$$

where $x_i(t) = (x_i^1(t), x_i^2(t), x_i^3(t))$ denotes the position of body i at time t, m_i is the mass of body i, and G is the gravitational constant.

As initial conditions we take the values at 00.00 GMT on January 1:st 2000, obtained from the US Naval Observatory with initial velocities obtained by fitting a high-degree polynomial to the values of December 1999. The initial data should be correct to five or more digits, which is similar to the available precision for the masses of the planets. We

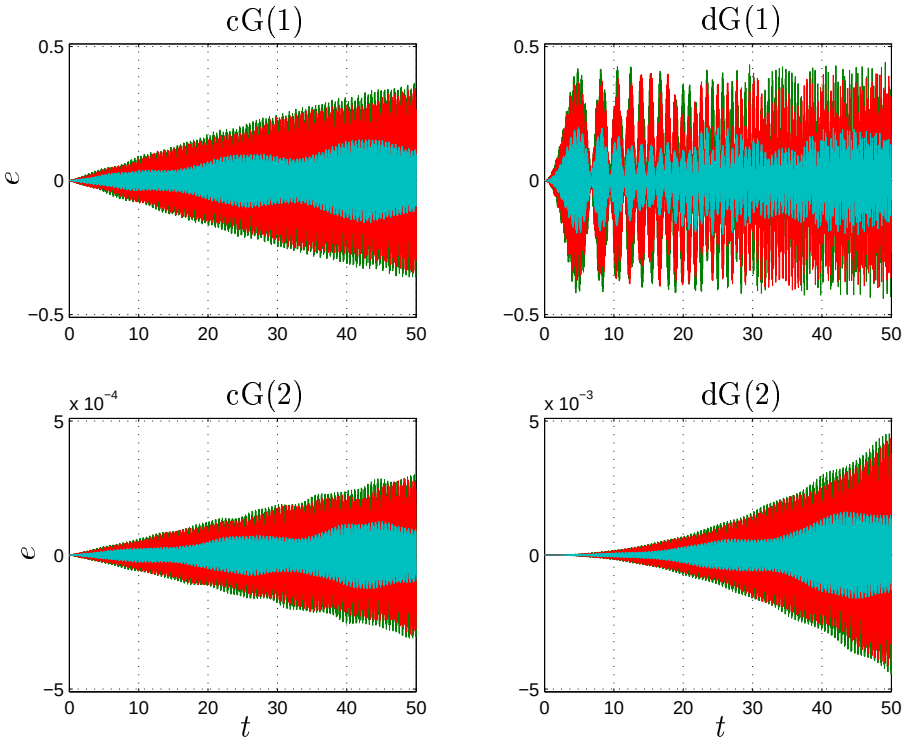

FIGURE 25. The growth of the error over 50 years for the Earth-Moon-Sun system as described in the text.

normalize length and time to have the space coordinates per astronomical unit, AU, which is (approximately) the mean distance between the Sun and Earth, the time coordinates per year, and the masses per solar mass. With this normalization, the gravitational constant is $4\pi^2$.

Investigating the *predictability* of the Solar System, the question is how far we can accurately compute the solution, given the precision in initial data. In order to predict the accumulation rate of errors, we solve the dual problem and compute stability factors. Assuming the initial data is correct to five or more digits, we find that the Solar System is computable on the order of 500 years. Including also the Moon, we cannot compute more than a few years. The dual solution grows linearly backward in time, see Figure 24, and so errors in initial data grow linearly with time. For every extra digit of increased precision, we thus reach ten times further.

We now touch briefly the fundamental question of the *computability* of the Solar System. Assuming correct initial data and model, we compute the trajectories for Earth, the Moon and the Sun over a time interval of 50 years using different methods. Since errors in initial data grow linearly, we expect stability factors for quadrature and round off to grow quadratically.

In Figure 25 we plot the errors for the 18 components of the solution, computed with time step $k = 0.001$ with $cG(1)$, $cG(2)$, $dG(1)$ and $dG(2)$. We see that the error seems to

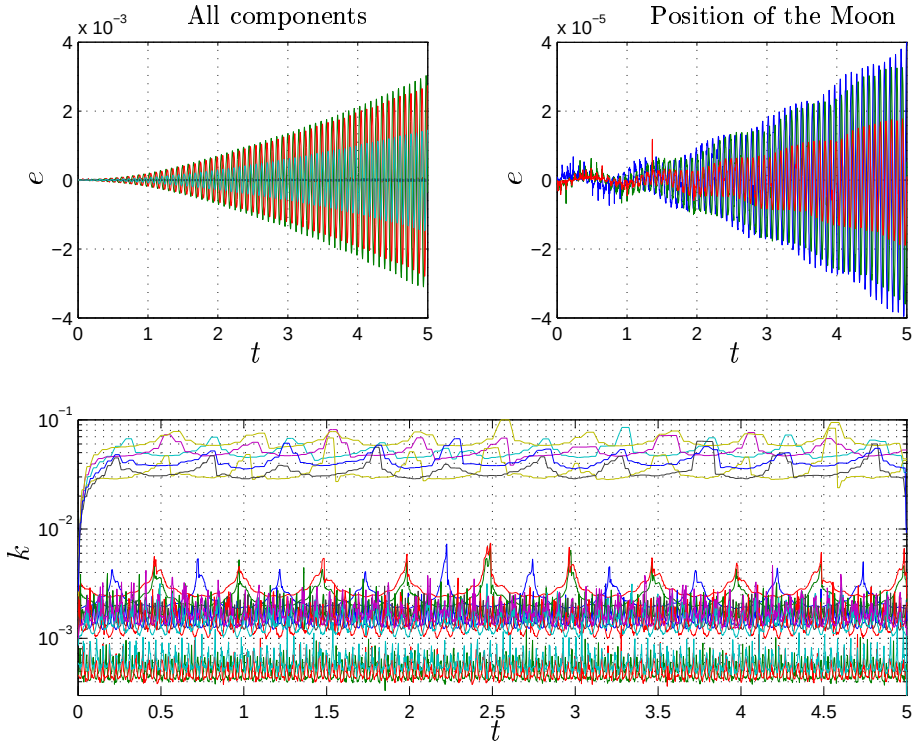

FIGURE 26. The growth of the error over 5 years for the Earth-Moon-Sun system computed with the mcG(2) method, together with the multi-adaptive time-steps.

grow linearly for $cG(q)$, which is in accordance with earlier observations [19] for periodic Hamiltonian systems, recalling that the $cG(q)$ conserves energy, [21]. The stability factors, however, grow quadratically and thus overestimate the error growth for this particular problem.

Examining the solutions obtained with the $dG(1)$ and $dG(2)$, we see that for these methods the error indeed grows quadratically. For the $dG(1)$ solution, the error reaches a maximum level of ~ 0.5 for the velocity components of the Moon. The error in position for the Moon is much smaller. This means that the Moon is still in orbit around Earth, the position of which is still very accurate, but the position relative to Earth is incorrect and thus also the velocity. The error thus grows quadratically until it reaches a limit. This effect is also visible for the error of the $cG(1)$ solution; the linear growth flattens out as the error reaches the limit. Notice also that even if the higher-order $dG(2)$ performs better on a short time-interval, it will be outrun on a long enough interval by the $cG(1)$ method with its linear accumulation of errors (for this particular problem).

Solving with the multi-adaptive method mcG(2), see Figure 26, the error grows quadratically because mcG(2) is not fully energy conserving. Computing in double precision the limit of computability seems to be $T \sim 10^6$.

15. Summary

We have presented aspects of computability of the non-stationary incompressible Navier Stokes equations with medium large Reynolds numbers. We have shown that computational solution of dual linearized problems is feasible and produces information on the growth and propagation of computational errors, which in particular may be used in adaptive error control and evaluation of computability of different mean values. We have also studied transition to turbulence computationally and discussed basic aspects of turbulence modeling based on scale similarity. Needless to say, these notes are preliminary with many open ends, which we hope to follow up in future work.

References

[1] R. Becker and R. Rannacher. (2001) An optimal control approach to a posteriori error estimation in finite element methods. Acta Numerica, pp 1-102.

[2] K. Eriksson, D. Estep, P. Hansbo and C. Johnson. (1995) Introduction to Adaptive Methods for Differential Equations. Acta Numerica, pp 105–158.

[3] K. Eriksson, D. Estep, P. Hansbo and C. Johnson. (1996) *Computational Differential Equations*, Cambridge University Press.

[4] K. Eriksson, D. Estep and C. Johnson. (2001) *Applied Mathematics: Body and Soul*, Springer.

[5] K. Eriksson, D. Estep, P. Hansbo, C. Johnson. *Advanced Computational Differential Equations*, to appear 2002.

[6] T.B Gatski, M. Y. Hussaini and J.L. Lumley. (1996) *Simulation and Modeling of Turbulent Flow*, Oxford Univ. Press.

[7] M. Giles, M. Larson, M. Levenstam and E. Süli. (1997) Adaptive error control for finite element approximations of the lift and drag coefficients in viscous flow, Technical Report NA-76/06, Oxford Univ. Computing Laboratory.

[8] M.Germano, U.Poimelli, P.Moin and W.Cabot. (1991) A dynamic subgrid scale eddy-viscosity model. Phys. Fluids A 3, 1760.

[9] J. Heywood, Remarks on the possible global regularity of solutions of the three-dimensional Navier-Stokes equations. Preprint, Univ of British Columbia.

[10] J. Hoffman, C. Johnson and S. Bertoluzza. (1999) Dynamic Subgrid Modeling I. Preprint. Chalmers Finite Element Center, to appear in Comp. Meth. Appl. Mech. Engrng.

[11] J. Hoffman. (2000) Dynamic Subgrid Modeling II. Preprint Chalmers Finite Element Center.

[12] J. Hoffman. (2001) Dynamic Subgrid Modeling for Convection-Diffusion Equations with Fractal Coefficients. *Multiscale and Multiresolution Methods*, Springer Lecture Series in Engineering, Springer Verlag.

[13] J. Hoffman. (2001) Dynamic Subgrid Modeling for Convection-Diffusion-Reaction Systems with Fractal solutions. to appear in International Journal for Numerical Methods in Fluids.

[14] D. Estep and C. Johnson. (1998) The pointwise computability of the Lorenz system. M^3AS 8, pp 1277-1306.

[15] C. Johnson, Finite Element Methods for Flow Problems, in Unstructured Grid Methods for Advection Dominated Flows, AGARD Report 787, 1992.

[16] C. Johnson, R. Rannacher and M. Boman (1995) On transition to turbulence and error control in CFD, Preprint 95-06, SFB 359, Univ. of Heidelberg.

[17] C. Johnson and R. Rannacher. (1995) Numerics and hydrodynamic stability: Towards error control in CFD, SIAM J. Numer. Anal., 32, pp 1058-1079.

[18] C. Johnson and R. Rannacher. (1994) On error control in CFD, Proc. Int. Workshop "Numerical Methods for the Navier-Stokes equations", Heidelberg Oct. 25-28, 1993, NNFM, Vol. 47, pp. 25-28, Vieweg, Braunschweig.
[19] M.G. Larson. (2000) Error Growth and A Posteriori Error Estimates for Conservative Galerkin Approximations of Periodic Orbits in Hamiltonian Systems M^3AS 10, pp 31-46.
[20] J. Leray. (1934) Sur le Mouvement d'un Liquide Visqueux Emplissent l'Espace, Acta Math. J 63, pp 193-248.
[21] A. Logg. (2001) Multi-Adaptive Galerkin Methods for ODEs I and II. Submitted to SIAM J. Sci. Comput.
[22] G.Papanicolau, K.Solna. (2001) Wavelet based estimation of local Kolmogorov turbulence. *Long-range Dependence Theory and Applications.* Birkhauser.
[23] R. Rannacher. (1999) Finite element methods for the incompressible Navier Stokes equations, Preprint Intsitute of Applied Mathematics, Univ. of Heidelberg.
[24] F.Sarghini, U.Piomelli, E.Balaras. (1999) Scale-similar models for large-eddy simulations. *Phys. Fluids* ***11****, 1596.*
[25] A.Scotti, C.Meneveau. Fractal dimension of velocity signal in high-Reynolds-number hydrodynamic turbulence. *Phys. Review E* ***51****, 5594*, 1995.
[26] P. Schmid and D. Henningson. (2001) *Stability and Transition in Shear Flows*, Applied Mathematical Sciences 142, Springer.
[27] G. Wagner and W.K. Liu. (1999) Turbulence simulation and multiple scale subgrid models, to appear in Computational Mechanics.

Chalmers Finite Element Center Preprints

2000–01 *Adaptive Finite Element Methods for the Unsteady Maxwell's Equations*
Johan Hoffman

2000–02 *A Multi-Adaptive ODE-Solver*
Anders Logg

2000–03 *Multi-Adaptive Error Control for ODEs*
Anders Logg

2000–04 *Dynamic Computational Subgrid Modeling (Licentiate Thesis)*
Johan Hoffman

2000–05 *Least-Squares Finite Element Methods for Electromagnetic Applications (Licentiate Thesis)*
Rickard Bergström

2000–06 *Discontinuous Galerkin Methods for Incompressible and Nearly Incompressible Elasticity by Nitsche's Method*
Peter Hansbo and Mats G. Larson

2000–07 *A Discountinuous Galerkin Method for the Plate Equation*
Peter Hansbo and Mats G. Larson

2000–08 *Conservation Properties for the Continuous and Discontinuous Galerkin Methods*
Mats G. Larson and A. Jonas Niklasson

2000–09 *Discontinuous Galerkin and the Crouzeix-Raviart element: Application to elasticity*
Peter Hansbo and Mats G. Larson

2000–10 *Pointwise A Posteriori Error Analysis for an Adaptive Penalty Finite Element Method for the Obstacle Problem*
Donald A. French, Stig Larson and Ricardo H. Nochetto

2000–11 *Global and Localised A Posteriori Error Analysis in the Maximum Norm for Finite Element Approximations of a Convection-Diffusion Problem*
Mats Boman

2000–12 *A Posteriori Error Analysis in the Maximum Norm for a Penalty Finite Element Method for the Time-Dependent Obstacle Problem*
Mats Boman

2000–13 *A Posteriori Error Analysis in the Maximum Norm for Finite Element Approximations of a Time-Dependent Convection-Diffusion Problem*
Mats Boman

2001–01 *A Simple Nonconforming Bilinear Element for the Elasticity Problem*
Peter Hansbo and Mats G. Larson

2001–02 *The $\mathcal{LL}^*$ Finite Element Method and Multigrid for the Magnetostatic Problem*
Rickard Bergström, Mats G. Larson, and Klas Samuelsson

2001–03 *The Fokker-Planck Operator as an Asymptotic Limit in Anisotropic Media*
Mohammad Asadzadeh

2001–04 *A Posteriori Error Estimation of Functionals in Elliptic Problems: Experiments*
Mats G. Larson and A. Jonas Niklasson

2001–05 *A Note on Energy Conservation for Hamiltonian Systems Using Continuous Time Finite Elements*
Peter Hansbo

2001–06 *Stationary Level Set Method for Modelling Sharp Interfaces in Groundwater Flow*
Nahidh Sharif and Nils-Erik Wiberg

2001–07 *Integration methods for the calculation of the magnetostatic field due to coils*
Marzia Fontana

2001–08 *Adaptive finite element computation of 3D magnetostatic problems in potential formulation*
Marzia Fontana

2001–09 *Multi-Adaptive Galerkin Methods for ODEs I: Theory & Algorithms*
Anders Logg

2001–10 *Multi-Adaptive Galerkin Methods for ODEs II: Applications*
Anders Logg

2001–11 *Energy norm a posteriori error estimation for discontinuous Galerkin methods*
Roland Becker, Peter Hansbo, and Mats G. Larson

2001–12 *Analysis of a family of discontinuous Galerkin methods for elliptic problems: the one dimensional case*
Mats G. Larson and A. Jonas Niklasson

2001–13 *Analysis of a nonsymmetric discontinuous Galerkin method for elliptic problems: stability and energy error estimates*
Mats G. Larson and A. Jonas Niklasson

2001–14 *A hybrid method for the wave equation*
Larisa Beilina, Klas Samuelsson, Krister Åhlander

2001–15 *A Finite Element Method for Domain Decomposition with Non-Matching Grids*
Roland Becker, Peter Hansbo and Rolf Stenberg

2001–16 *Application of stable FEM-FDTD hybrid to scattering problems*
Thomas Rylander and Anders Bondeson

2001–17 *Eddy current computations using adaptive grids and edge elements*
Y. Q. Liu, A. Bondeson, R. Bergström, C. Johnson, M. G. Larson, and K. Samuelsson

2001–18 *Adaptive finite element methods for incompressible fluid flow*
J. Hoffman, C. Johnson

2001–19 *Dynamic subgrid modeling for time dependent convection–diffusion–reaction equations with fractal solutions*
J. Hoffman

These preprints can be obtained from

`www.phi.chalmers.se/preprints`